Advances in Differential Equations and Control Processes 2026, 33(3), 4372.
doi: https://doi.org/10.59400/adecp4372

Article

Nonlinear dynamic response and time-delay feedback vibration control of multilayer beams on compressible clayey foundations subjected to moving concentrated loads

Roger Eno[1], Guillaume Hervé Poh'sié[2,3,4], Hermann Joel Ouandji Boutcheng[5], Ekoum Ewandjo Nkoue[1], Dianorre Tokoue Ngatcha[1], Joseph Mousi Bikoun[1,6], Fabien Kenmogne[6,*], Séverin Nguiya[7]

[1] Laboratory for Mechanics and Materials (LMEMA), Department of Civil Engineering, National Higher Polytechnic School of Douala, University of Douala, Douala P.O. Box 2701, Cameroon; enoroger6@gmail.com (RE); cedrickekoum@yahoo.com (EEN); tokouengatcha1@gmail.com (DTN); josephbikoun@gmail.com (JMB)
[2] Department of Civil Engineering, Higher Institute of Advanced Technologies (ISTA), University Institute of the Gulf of Guinea (IUG), Douala P.O. Box 12489, Cameroon; guillaume.herve@ubuea.cm
[3] Department of Mechanical Engineering, College of Technology, University of Buea, Buea P.O. Box 63, Cameroon
[4] Department of Civil Engineering, National Higher Polytechnic School of Yaoundé, University of Yaoundé I, Yaoundé P.O. Box 8390, Cameroon
[5] Department of Physics, Faculty of Science, University of Buea, Buea P.O. Box 63, Cameroon; hermannjoel74@gmail.com
[6] Department of Civil Engineering, Advanced Teacher Training College for Technical Education (ENSET), University of Douala, Douala P.O. Box 1872, Cameroon
[7] Laboratory for Geophysics (LG), National Higher Polytechnic School of Douala, University of Douala, Douala P.O. Box 2701, Cameroon; nguiyaplus@yahoo.fr
* **Corresponding authors:** Fabien Kenmogne, kenfabien@yahoo.fr

CITATION

Eno R, Poh'sié GH, Boutcheng HJO, et al. Nonlinear dynamic response and time-delay feedback vibration control of multilayer beams on compressible clayey foundations subjected to moving concentrated loads. Advances in Differential Equations and Control Processes. 2026; 33(3): 4372. https://doi.org/10.59400/adecp4372

ARTICLE INFO

Received: 7 May 2026
Revised: 15 July 2026
Accepted: 22 July 2026
Available online: 16 August 2026

Abstract: This study investigates the nonlinear vibration behaviour of multilayer beams resting on a compressible elastic foundation and subjected to a moving concentrated load. The objective is to analyse the combined effects of geometric nonlinearity, interlayer elastic coupling, foundation compressibility, and moving-load excitation on the dynamic response of the structure. An analytical formulation based on the Lagrangian formalism is developed, incorporating kinetic energy, bending energy, foundation stiffness, interlayer coupling, and nonlinear stretching effects. The proposed formulation captures the structural dynamics through coupled Duffing-type nonlinear modal interactions, while accounting for damping and moving-load excitation. A Fourier-Galerkin modal reduction is employed to derive a reduced-order temporal system, whose equilibrium states and stability characteristics are investigated. Numerical simulations performed using Fourier modal decomposition and a fourth-order Runge-Kutta scheme reveal complex dynamic behaviours, including multistability, resonance amplification, quasi-periodic oscillations, and branch-jump phenomena induced by nonlinear interactions and parameter sensitivity. To mitigate excessive vibrations, a time-delay feedback controller is introduced and applied to all modal coordinates. The delayed control law yields a transcendental characteristic equation, from which explicit stability conditions are established in terms of the feedback gain and time delay. Numerical results demonstrate that the proposed controller effectively suppresses nonlinear vibration amplification, reduces oscillation amplitudes, and improves the dynamic stability of the system. The proposed framework provides a comprehensive nonlinear beam-foundation interaction model combined with delay-based vibration control, contributing to the analysis and stabilization of multilayer structural systems subjected to moving loads on deformable foundations.

Keywords: moving concentrated load; multilayer beam; interlayer coupling; modal mismatch; dynamic control

1. Introduction

Structures subjected to moving loads on compressible soils, such as bridges, railways, and industrial platforms, are common in transportation infrastructure. Their dynamics are often complex, especially when these structures are multi-layered. One of the main challenges lies in accounting for the nonlinear effects of the structural materials, such as beams, and interactions with the soil. In the case of clayey soils, particularly characterized by pronounced nonlinear properties and dissipative behaviour, dynamic analysis becomes even more complex. Compressible clayey soils generally exhibit characteristics that significantly affect the dynamic behaviour of structures resting on them. Understanding the interaction between the multi-layer beam and the compressible soil is therefore crucial for analyzing the stability and vibration response of such structures subjected to mobile loads [1,2].

Despite advances in the study of structural vibrations under moving loads, relatively few studies have focused on the interaction between multilayer beams and compressible clayey soils, especially when nonlinear soil behaviour is considered. Moreover, the phenomena of resonance, bistability, and branch-jumps in these systems have not been widely explored. The non-linear dynamics generated by these phenomena can lead to structural instabilities and failures if not properly considered, as indicated by Elhuni and Basu [1], who studied the dynamic interaction between beams and nonlinear soils, and Karami and Ghayesh [3], who addressed moving loads on multi-layer microplates. Furthermore, research such as that of Li et al. [4] on the nonlinear vibrations of composite beams on elastic foundations demonstrates the importance of considering the effect of nonlinearities in the analysis of soil-structure interactions.

The work of Ter-Martirsyan et al. [5] proposed a method for analyzing the vibrations of submerged foundations in multi-layered soils with nonlinear and rheological properties, which sheds light on the effects of these properties on structural dynamics. Mourya et al. [6] also proposed approaches to better understand the effects of nonlinearity in soil-structure interactions for structures subjected to moving loads. Other studies, such as those of Zhai et al. [7] on train-rail-bridge interactions and flexibility constraints, highlight the complexity of multi-layer systems subjected to dynamic loads. The research of Youzera et al. [8], focusing on sandwich beams and nonlinear damping, also demonstrated the importance of considering these effects in the dynamic management of structures subjected to periodic loads. Kampitsis and Sapountzakis [9] studied beams subjected to dynamic loads on nonlinear foundations, demonstrating the impact of nonlinearities on the vibration responses of structures. Poudel and Chaulagain [10] investigated nonlinear soil–structure interaction, providing a useful basis for understanding the effects of compressible soils on the response of multi-layer structures.

The nonlinear phenomena induced by moving loads, soil compressibility, and interlayer interactions may generate excessive vibration amplitudes, resonance amplification, and dynamic instabilities, which can adversely affect the structural performance and serviceability of engineering systems. Consequently, the development of efficient vibration-control strategies has become an important research topic. Several approaches have been proposed in the literature, including linear quadratic regulators (LQRs) and active tuned mass devices (ATMDs) for multilayer beam structures [11]. Other studies have also demonstrated the effectiveness of active-control techniques in mitigating vibrations in nonlinear and complex structural systems [4, 7]. Nevertheless, the application of time-delay feedback control to multilayer beam-soil systems subjected to moving concentrated loads remains largely unexplored. Existing studies have primarily investigated beam-foundation interaction [1, 4, 10], multilayer structural dynamics [3, 7, 8], and vibration-control strategies [11] as separate research topics. Consequently, the combined effects of soil compressibility, interlayer elastic coupling, geometric nonlinearities, moving-load excitation, and delayed feedback control on the dynamic behaviour of multilayer beam systems remain insufficiently understood. To address this issue, the present study develops a nonlinear beam-soil interaction model that accounts simultaneously for these mechanisms. The resulting coupled modal equations provide a framework for analysing equilibrium states, resonance amplification, multistability, branch-jump phenomena, and quasi-periodic responses. Furthermore, a time-delay feedback controller is incorporated, and its stability properties are investigated through the associated characteristic equation. This approach enables a unified analysis of both the nonlinear dynamic response and vibration stabilization of multilayer beam systems resting on compressible soils and subjected to moving concentrated loads.

This investigation is devoted to understanding the nonlinear vibration response and control of multilayer beams interacting with compressible soil under moving concentrated loading. The study pursues the following objectives:

- To develop the governing equations of the multilayer beam-soil system by taking into account damping and geometric nonlinearities;
- To analyse the equilibrium states and stability of the nonlinear system;
- To investigate periodic, quasi-periodic and multistable responses under moving-load excitation;
- To design and assess a time-delay feedback controller for vibration suppression and system stabilization.

The remainder of the manuscript is organized as follows. Section 2 presents the mathematical model and governing equations for the multilayer beam system, including the physical configuration, energy and Lagrangian formulations, and modal reduction. Section 3 develops the analytical formulation, including the equilibrium solutions, stability analysis, and multiple-scale analysis for two- and three-layer beam configurations. Section 4 presents the numerical results, including frequency–amplitude responses, temporal evolutions, phase portraits, Fourier spectra, and the effects of excitation frequency, input amplitude, and the number of beam layers. This section also includes the formulation and stability analysis of the time-delay feedback controller, together with its numerical verification and a discussion of the main results. Finally, Section 5 summarises the study's main findings and presents its limitations and perspectives for future research.

2. Mathematical model

2.1. Physical configuration

The structural system examined in this study is composed of several superposed beam layers mechanically connected by continuous viscoelastic interfaces, as illustrated in **Figure 1**. A concentrated load travelling at constant speed provides the external excitation responsible for the structural vibrations, whereas the multilayer beam–foundation assembly represents the mechanical system analysed. This configuration is representative of several engineering applications. In railway infrastructures, the beam layers may represent the rails supported by a multilayer foundation through ballast and subgrade components, while the travelling force models the passage of a train, following the physical interpretation proposed by Eno et al. [2]. Similar modelling assumptions can also be adopted for highway bridges subjected to heavy moving vehicles or for pavement systems experiencing the action of rolling compaction equipment [12]. In these situations, the moving body of mass M generates a travelling mechanical excitation acting on the structural system.

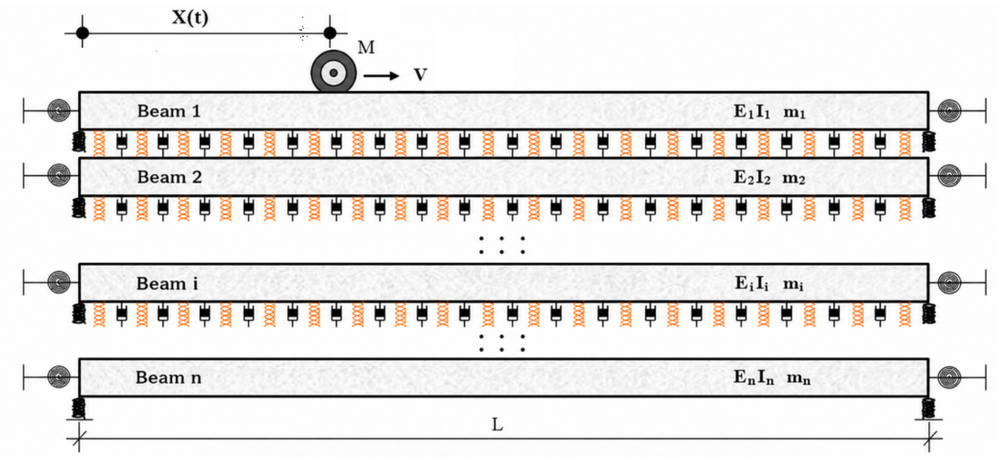

Figure 1. Schematic representation of the multilayer beam system with viscoelastic interlayer connections.

2.2. Governing formulation

The mechanical configuration depicted in **Figure 1** is modelled as a multilayer beam assembly composed of N Euler–Bernoulli beam members linked by continuously distributed viscoelastic connectors. Each beam is assumed to possess uniform geometric and material properties along the span L. Nevertheless, the deformable interlayer connections allow relative displacements between adjacent layers, thereby introducing coupling effects into the structural response. To establish the governing formulation, the total mechanical energy of the assembly is expressed as the sum of the kinetic energy, the elastic bending energy of each beam, the deformation energy stored in the viscoelastic interfaces, the strain energy associated with the supporting foundation, and the energy contribution arising from geometric nonlinear stretching.

2.2.1. Translational kinetic energy

Because the beam layers are assumed to be slender, the contribution of rotary inertia is disregarded in the present formulation. Under this assumption, the translational motion energy associated with the multilayer system is expressed as [13,14]:

$$T = \frac{1}{2} \sum_{i=1}^{N} \rho_i A_i \int_0^L \left(\frac{\partial w_i(x,t)}{\partial t} \right)^2 dx, \tag{1}$$

where ρ_i $\left(\mathrm{kg/m^3}\right)$ denotes the material density of the i^{th} layer, A_i is its cross-sectional area, and $m_i = \rho_i A_i$ represents the corresponding mass per unit length. The variable L denotes the span of the beam, whereas $w_i(x,t)$ defines the vertical deflection of layer i at the longitudinal coordinate *x* and time *t*. To describe the interaction between the beam and the supporting soil, the classical Winkler foundation idealization is adopted. Within this framework, the supporting medium is represented by a continuous distribution of uncoupled linear springs. Consequently, the reaction developed by the foundation at any location depends exclusively on the displacement at that same location, with no interaction between neighbouring points [13,15,16].

2.2.2. Elastic energy contributions

❖ **Energy associated with flexural deformation**

The elastic energy stored in the i^{th} beam layer as a result of flexural deformation is expressed by:

$$V_{\text{bend}} = \frac{1}{2} \sum_{i=1}^{N} E_i I_i \int_0^L \left(\frac{\partial^2 w_i(x,t)}{\partial x^2} \right)^2 dx, \tag{2}$$

Where $I_i = \iint_{A_i} z^2 dydz$ is the second moment of the cross-section and E_i is Young's modulus for layer *i*.

❖ **Interlayer coupling energy**

The mechanical interaction between adjacent beam layers is represented through continuously distributed elastic connectors. The corresponding energy contribution is formulated as:

$$V_{\text{coupling}} = \frac{1}{2} \sum_{i=1}^{N} \sum_{j=1}^{N} \gamma_{ij} \int_0^L \left(w_i(x,t) - w_j(x,t) \right)^2 dx, \tag{3}$$

In which γ_{ij} ($\mathrm{N/m^2}$) denotes the stiffness of the elastic connection established between layers *i* and j, while the quantity $w_i(x,t) - w_j(x,t)$ represents their relative transverse displacement.

❖ **Nonlinear stretching potential energy**

Large transverse deflections induce axial stretching in each beam layer, thereby introducing an additional nonlinear strain-energy contribution. This contribution is represented by:

$$V_{\text{stretch}} = \frac{1}{2} \sum_{i=1}^{N} \frac{E_i A_i}{2L_i} \left(\frac{1}{2} \int_0^L \left(\frac{\partial w_i(x,t)}{\partial x} \right)^2 dx \right)^2, \tag{4}$$

Where A_i ($\mathrm{m^2}$) denotes the initial cross-sectional area of the i^{th} beam layer, E_i is the corresponding Young's modulus, and L_i represents the undeformed beam length.

To model the soil-structure interaction, the Winkler foundation model [17] is adopted. In this approach, the foundation is represented by a set of independent vertical springs, such that the soil reaction at a given point is proportional to the local displacement and independent of the neighbouring points. The foundation of layer *i* is characterized by a constant spring modulus K_{fi}, leading to the following elastic potential energy:

❖ **Foundation potential energy (Winkler model)**

$$V_{\text{foundation}} = \frac{1}{2}\sum\nolimits_{i\,=\,1}^{N}\int_0^L K_{fi}\left(w_i(x,t)\right)^2 dx, \tag{5}$$

Where K_{fi} (N/m^2) is the stiffness coefficient related to soil parameters as [14,17].

$$K_{fi} = \frac{0.65E_s}{1-v^2}\left(\frac{E_sB^4}{E_iI_i}\right)^{\frac{1}{12}}, \tag{6}$$

Where *B* is the width, E_s is Young's modulus of the soil, and v (ranging between $0 < v < 0.45$) is the Poisson's ratio of the soil. E_i is the Young's modulus of the beam material, I_i is the second moment of area of the beam cross-section, and E_iI_i represents the flexural rigidity of the beam. Equation (6) corresponds to an empirical Winkler foundation modulus commonly used for shallow beams resting on compressible soils. The expression provides an equivalent foundation stiffness obtained from the interaction between beam rigidity and soil elasticity.

❖ **Work of the moving load**

Consider a concentrated load travelling along the beam with a constant velocity V. Its instantaneous position is defined by the kinematic relation $x_0(t) = Vt$. The generalized work associated with this travelling force is represented by [14]:

$$V_{\text{load}} = -\sum\nolimits_{i\,=\,1}^{N}\int_0^L p(x,t)w_i(x,t)dx, \tag{7}$$

In which $p(x,\ t) = P_0(t)\delta\left(x-x_0\right)\ \delta_{i1}$. Here, P_0 = Mg denotes the gravitational force generated by the moving mass M, with g representing the gravitational acceleration. The Dirac distribution $\delta\left(x-x_0\right)$ localizes the external force at the instantaneous position x_0, whereas the discrete indicator δ_{i1} specifies that the excitation is applied exclusively to the first beam layer.

2.2.3. Lagrange formulation

The system dynamics are formulated through the following Lagrangian function [13,14]:

$$L = T - \left(V_{\text{bend}} + V_{\text{coupling}} + V_{\text{stretch}} + V_{\text{foundation}} + V_{\text{load}}\right), \tag{8}$$

This equation is the expanded version of (8), which includes all the energy terms explicitly in integral form, leading to:

$$L = \frac{1}{2}\ \sum_{i\,=\,1}^{N} \int_0^L dx\, [\rho_i A_i \left(\frac{\partial w_i(x,t)}{\partial t}\right)^2 - E_i I_i\ \left(\frac{\partial^2 w_i(x,t)}{\partial x^2}\right)^2$$
$$-K_{fi}\,(w_i(x,t))^2 + 2P_0\ w_i(x,t)\delta\,(x-x_0)\,\delta_{i1} - \tag{9}$$
$$\sum_{j\,=\,1}^{N} \gamma_{ij}\,(w_i(x,t) - w_j(x,t))^2] - \ \sum_{i\,=\,1}^{N} \frac{E_i A_i}{2L_i}\ \left(\frac{1}{2}\int_0^L \left(\frac{\partial w_i(x,t)}{\partial x}\right)^2 dx\right)^2.$$

Real engineering structures inevitably dissipate part of their mechanical energy through internal and external damping mechanisms. To account for these irreversible losses, the damping effects are incorporated into the formulation by means of the Rayleigh dissipation function, expressed as [14]:

$$F_D(w) = \frac{1}{2}\sum_{i\,=\,1}^{N} \mu_i \int_0^L \left(\frac{\partial w_i(x,t)}{\partial t}\right)^2 dx, \tag{10}$$

Where μ_i is the viscous damping coefficient of layer *i*. Application of the Euler–Lagrange formalism to the proposed system yields the governing equations of motion [13,14]:

$$\frac{\partial}{\partial t}\left(\frac{\partial L}{\partial \dot{w}_i}\right) - \frac{\partial L}{\partial w_i} + \frac{\partial}{\partial x}\left(\frac{\partial L}{\partial w_i'}\right) - \frac{\partial^2}{\partial x^2}\left(\frac{\partial L}{\partial w_i''}\right) = -\frac{\partial F_D}{\partial \dot{w}_i}, \tag{11}$$

2.2.4. Motion equations for the non-dissipative linear case

System of partial motion equations

For this particular case, $F_D = 0$ and the nonlinear stretching contribution V_{stretch} is omitted, meaning that the last term cancels in Equation (9) and the second member of the variational Equation (11). Let us now assume that the system is under localized loading, meaning that $P(x,t) = P_0\delta\,(x - \mathrm{x}_0)\,\delta_{i1}$. Applying the Euler–Lagrange Equation (11) to the expanded Lagrangian expressed in Equation (9), and evaluating the corresponding variational derivatives, yields the governing partial differential equations of the multilayer beam system:

$$m_i\ddot{w}_i + K_{fi}w_i + \sum_{j\,=\,1}^{N} \gamma_{ij}(w_i - w_j) + E_i I_i w_{ixxxx} - p(x,t)\delta_{i1} = 0, \tag{12}$$

Where $\rho_i A_i = m_i$ is the linear mass kg/m and $\ddot{w}_i$: acceleration in $\left(\mathrm{m/s}^2\right)$. The introduction of δ_{i1} is justified by the fact that the load is applied at the entrance (first beam, *i* = 1). This set of Equation (12) can be written in the following expanded form:

$$\begin{cases} m_1\ddot{w}_1 + K_{f1}w_1 + \sum\limits_{j\,=\,1}^{N} \gamma_{1j}(w_1 - w_j) + E_1 I_1 \frac{\partial^4 w_1}{\partial x^4} = p(x,t), \\ m_2\ddot{w}_2 + K_{f2}w_2 + \sum\limits_{j\,=\,1}^{N} \gamma_{2j}\,(w_2 - w_j) + E_2 I_2 \frac{\partial^4 w_2}{\partial x^4} = 0. \\ m_3\ddot{w}_3 + K_{f3}w_3 + \sum\limits_{j\,=\,1}^{N} \gamma_{3j}\,(w_3 - w_j) + E_3 I_3 \frac{\partial^4 w_3}{\partial x^4} = 0, \\ \cdots \\ m_N\ddot{w}_N + K_{fN}w_N + \sum\limits_{j\,=\,1}^{N} \gamma_{Nj}\,(w_N - w_j) + E_N I_N \frac{\partial^4 w_N}{\partial x^4} = 0. \end{cases} \tag{13}$$

2.2.5. System of differential equations governing the temporal part

Let us seek the solution of Equation (13) for the homogeneous case in the form of a standing wave: $w_i(x,t) = q_i(t)\phi(x)$, assuming that the interaction between two beams acts mainly on the temporal component and is negligible on the spatial component, this assumption being valid when the interlayer stiffness remains moderate compared with the bending stiffness of each beam, allowing the mode shapes to remain close to those of uncoupled simply supported beams. This transforms Equation (12) into the following form:

$$\left[m_i\ddot{q}_i + K_{fi}q_i + \sum\nolimits_{j\,=\,1}^{N} \gamma_{ij}\left(q_i - q_j\right)\right]\phi(x) + E_iI_iq_i(t)\frac{\partial^4}{\partial x^4}\phi(x) = 0. \qquad (14)$$

For the homogeneous problem, Equation (14) can be separated into spatial and temporal parts as follows:

$$\begin{cases} \left[m_i\ddot{q}_i + K_{fi}q_i + \sum_{j\,=\,1}^{N} \gamma_{ij}\left(q_i - q_j\right)\right] + E_iI_ik^4q_i(t) = 0, \\ \frac{\partial^4}{\partial x^4}\phi(x) = k^4\phi(x). \end{cases} \qquad (15)$$

where k is a constant defining the modal wavenumber. The spatial part of this equation admits the solution

$$\phi(x) = A_1\sin(kx) + A_2\cos(kx) + A_3\exp(kx) + A_4\exp(-kx). \qquad (16)$$

where A_1, A_2, A_3, and A_4 are integration constants determined from the boundary conditions. For a beam of length L simply supported at both ends, and in order to ensure the mathematical admissibility of the modal decomposition, the transverse displacement field is assumed to belong to the Hilbert space

$$V = \left\{\phi \in H^2(0,L);\ \phi(0) = \phi(L) = 0,\ \text{and}\ \frac{\partial^2}{\partial x^2}\phi(0) = \frac{\partial^2}{\partial x^2}\phi(L) = 0\right\}, \qquad (17)$$

which thus satisfies the simply supported boundary conditions: where L represents the beam length in the considered spatial domain. These conditions lead to

$$A_2 = A_3 = A_4 = 0,\ \text{and}\ k = \frac{n\pi}{L};\, n = 1, 2, \ldots, \infty,\ \text{and}\ \phi_n(x) = \sin\left(\frac{n\pi}{L}x\right), \qquad (18)$$

Which forms a complete orthogonal basis of $\left(L^2(0,L)\right)$. n here is the modal number. Therefore, any admissible displacement field can be represented through the Fourier modal expansion $W_i(x,t) = \sum_{n\,=\,1}^{\infty} q_{ni}(t)\phi_n(x)$, The convergence of this expansion is guaranteed in the $L^2(0,L)$ sense by the completeness of the eigenfunctions. Furthermore, for sufficiently smooth displacement fields, the convergence is uniform. This property justifies the modal projection procedure. Let us suppose that the beam is subjected to a concentrated load applied at position x_0, the external excitation can be written as

$$p(x,t) = \frac{2}{L}\sum\nolimits_{n\,=\,1}^{\infty}\int_0^L p(\zeta,t)\sin\left(\frac{n\pi}{L}\zeta\right)\sin(\frac{n\pi}{L}x)d\zeta. \qquad (19)$$

Assume now that the system is subjected to a concentrated load: $p(x,t) = P_0\delta\left(x-x_0\right)$, leading to $p(x,t) = \frac{2P_0}{L}\sum_{n=1}^{\infty}\sin\left(\frac{n\pi}{L}x_0\right)\sin(\frac{n\pi}{L}x)$. Substituting this expression into the governing equation and applying the orthogonality properties of the mode shapes yields the corresponding system of modal equations:

$$\begin{cases} m_1\ddot{q}_1 + \left(K_{f1} + \frac{E_1I_1n^4\pi^4}{L^4}\right)q_1 + \sum_{j=1}^{N}\gamma_{1j}(q_1 - q_j) = \frac{2P_0}{L}\sin\left(\frac{n\pi x_0}{L}\right) \\ m_2\ddot{q}_2 + \left(K_{f2} + \frac{E_2I_2n^4\pi^4}{L^4}\right)q_2 + \sum_{j=1}^{N}\gamma_{2j}\left(q_2 - q_j\right) = 0, \\ m_3\ddot{q}_3 + \left(K_{f3} + \frac{E_3I_3n^4\pi^4}{L^4}\right)q_3 + \sum_{j=1}^{N}\gamma_{3j}\left(q_3 - q_j\right) = 0, \\ \ldots \\ m_N\ddot{q}_N + \left(K_{fN} + \frac{E_NI_Nn^4\pi^4}{L^4}\right)q_N + \sum_{j=1}^{N}\gamma_{Nj}\left(q_N - q_j\right) = 0 \end{cases}, \quad (20)$$

3. Analytical solution and stability

3.1. Steady-state response

The steady-state behaviour of the multilayer beam system is obtained by seeking time-independent solutions of the nonlinear governing equations. This procedure leads to the following equilibrium system: $Aq_0 = B$, $q_0 = [q_{01}, q_{02}, \ldots q_{0N}]$, $B = [\frac{2}{L}P_0\sin\left(\frac{n\pi}{L}x_0\right),\ 0,\ 0,\ldots]$ and

$$A = \begin{vmatrix} \Gamma_1 & -\gamma_{12} & .. & -\gamma_{1N} \\ -\gamma_{21} & \Gamma_2 & .. & -\gamma_{2N} \\ .. & .. & .. & .. \\ -\gamma_{N1} & -\gamma_{N2} & .. & \Gamma_N \end{vmatrix}, \quad (21)$$

Where the coefficients are defined as: $\Gamma_i = K_{fi} + E_iI_i\frac{n^4\pi^4}{L^4} + \sum_{j\neq i}^{N}\gamma_{ij}$. The equilibrium solution is therefore obtained as: $q_0 = A^{-1}B$. For a two-layer beam system (N = 2), the equilibrium modal coordinates reduce to:

$$\begin{cases} q_{01} = \frac{2P_0\Gamma_2}{L(\Gamma_1\Gamma_2-\gamma_{12}\gamma_{21})}\sin\left(\frac{n\pi}{L}x_0\right), \\ q_{02} = \frac{2P_0\gamma_{21}}{L(\Gamma_1\Gamma_2-\gamma_{12}\gamma_{21})}\sin\left(\frac{n\pi}{L}x_0\right). \end{cases} \quad (22)$$

By taking into account this set of solutions into the original variable as defined above, one obtains the following envelope of the signal:

$$\begin{cases} w_1(x) = \sum_{n=1}^{N}\frac{2P_0\Gamma_2}{L(\Gamma_1\Gamma_2-\gamma_{12}\gamma_{21})}\sin\left(\frac{n\pi}{L}x_0\right)\sin\left(\frac{n\pi}{L}x\right), \\ w_2(x) = \sum_{n=1}^{N}\frac{2P_0\gamma_{21}}{L(\Gamma_1\Gamma_2-\gamma_{12}\gamma_{21})}\sin\left(\frac{n\pi}{L}x_0\right)\sin\left(\frac{n\pi}{L}x\right). \end{cases} \quad (23)$$

For N = 3, we have the equilibrium points:

$$q_{01} = \frac{2P_0}{L}\left(\frac{\Gamma_2\Gamma_3 - \gamma_{23}\gamma_{32}}{\Delta}\right)\sin\left(\frac{n\pi}{L}x_0\right), q_{02} = \frac{2P_0}{L}\left(\frac{\gamma_{21}\Gamma_3 + \gamma_{23}\gamma_{31}}{\Delta}\right)\sin\left(\frac{n\pi}{L}x_0\right),$$
$$q_{03} = \frac{2P_0}{L}\left(\frac{\gamma_{21}\Gamma_2 + \gamma_{12}\gamma_{31}}{\Delta}\right)\sin\left(\frac{n\pi}{L}x_0\right), \quad (24)$$
$$\Delta = \Gamma_1\Gamma_2\Gamma_3 + \gamma_{12}\gamma_{23}\gamma_{31} + \gamma_{13}\gamma_{21}\gamma_{32} - \Gamma_1\gamma_{23}\gamma_{32} - \Gamma_2\gamma_{13}\gamma_{31} - \Gamma_3\gamma_{12}\gamma_{21}.$$

Δ denotes the determinant of the coefficient matrix. For the homogeneous solution in the sinusoidal form, one has the following dispersion relation:

$$\det\left[\left(-\mathrm{m}_i\omega^2+\Gamma_i\right)\mathrm{q_i}-\sum\nolimits_{\mathrm{j}\,\neq\,\mathrm{i}}^{\mathrm{N}}\gamma_{ij}\mathrm{q_j}\right]=0. \tag{25}$$

Particularly for N = 2, we obtain:

$$\omega^2=\frac{1}{2}\left(\frac{\mathrm{m_1}\Gamma_2\;+\;\mathrm{m_2}\Gamma_1\;\pm\;\sqrt{(\mathrm{m_1}\Gamma_2\;-\;\mathrm{m_2}\Gamma_1)^2\;+\;4\mathrm{m_1m_2}\gamma_{12}\gamma_{21}}}{\mathrm{m_1m_2}}\right). \tag{26}$$

For N = 3, we get the dispersion relation:

$$\omega^6-a_1\omega^4+a_2\omega^2+a_3=0; \tag{27}$$

with

$$\begin{gathered}a_1=\sum\nolimits_{i\,=\,1}^{3}\frac{\Gamma_i}{m_i}\,,a_2=\sum\nolimits_{\substack{i,j,k\;=\;1\\ i\;\neq\;j\;\neq\;k}}^{3}\frac{\Gamma_j\Gamma_k\,+\,\gamma_{jk}\gamma_{kj}}{m_i},\\ a_3=\frac{1}{m_1m_2m_3}\left[\sum\nolimits_{\substack{\mathrm{i,\,j,\,k}\,=\,1\\ i\neq j\neq k}}^{3}\left(\Gamma_\mathrm{i}\gamma_\mathrm{jk}\gamma_\mathrm{kj}-\gamma_\mathrm{ij}\gamma_\mathrm{jk}\gamma_\mathrm{ki}\right)-\Gamma_1\Gamma_2\Gamma_3\right],\end{gathered} \tag{28}$$

which can be solved using the Cardan method as follows:

$$\begin{gathered}\omega_1^2=\frac{a_1}{3}+A_++A_-,\;\omega_{2,3}^2=\frac{a_1}{3}-\frac{1}{2}\left(A_++A_-\right)\pm\frac{i\sqrt{3}}{2}\;\left(A_+-A_-\right),\\ A_\pm^3=-\frac{q}{2}\pm\sqrt{\Delta}\\ \Delta=\frac{q^2}{2}+\frac{p^3}{3},p=a_2-\frac{a_1^2}{3},q=\frac{2a_1^3}{27}-\frac{a_1a_2}{3}+a_3\end{gathered} \tag{29}$$

3.2. Nonlinear dissipative dynamic formulation

3.2.1. Temporal governing equations

To reduce the governing partial differential equations to a system of ordinary differential equations, the transverse displacement of each beam layer is approximated by a separable representation of the form: $w_i(x,t)=\phi(x)q_i(t)$, where $\phi(x)$ denotes the spatial mode shape, which is a bounded function satisfying the boundary conditions, while $q_i(t)$ represents the temporal part. Substituting this equation into the Lagrangian Equation (9), leads to the following expression:

$$\begin{gathered}L=\frac{1}{2}\sum\nolimits_{i\,=\,1}^{N}[m_i\dot{q}_i^2(t)\int_0^L\phi^2(x)dx-(E_iI_i\int_0^L(\frac{\partial^2\phi(x)}{\partial x^2})^2dx+\\ K_{fi}\int_0^L\phi^2(x)dx)q_i^2(t)+2P_0q_i(t)\int_0^L\phi(x)\delta(x-Vt)dx-\\ \sum\nolimits_{j\,=\,1}^{N}\gamma_{ij}\left(q_i(t)-q_j(t)\right)^2\int_0^L\phi^2(x)dx\;-\frac{E_iA_i}{4L_i}q_i^4(t)(\int_0^L(\frac{\partial\phi(x)}{\partial x})^2dx)^2],\end{gathered} \tag{30}$$

The Rayleigh dissipation function in modal form is then given by:

$$F_D=\frac{1}{2}\sum\nolimits_{i\,=\,1}^{N}\mu_{ir}\dot{q}_i^2(t)\int_0^L\phi^2(x)dx, \tag{31}$$

In the above equations, the terms $\int_0^L \phi^2(x)dx$, and $\int_0^L \left(\frac{\partial^2\phi(x)}{\partial x^2}\right)^2 dx$ are constant parameters, while according to delta function properties $\int_0^L \phi(x)\delta\left(x-x_0\right)dx = \phi\left(x_0\right),\ x_0 = Vt.$ We can thus rewrite the Lagrangian formulation as:

$$\frac{\partial}{\partial t}\left(\frac{\partial L}{\partial \dot{q}_i}\right) - \frac{\partial L}{\partial q_i} = -\frac{\partial F_D}{\partial \dot{q}_i}. \tag{32}$$

In the present work, only the first vibration mode is retained through a Galerkin truncation procedure. This approximation is commonly adopted in nonlinear beam dynamics because the fundamental mode generally carries the largest proportion of the vibration energy and dominates the structural response under moderate excitation levels [18]. Higher-order modes mainly contribute to local high-frequency responses and have a limited influence on the global nonlinear behaviour investigated in this study. This leads to the following damped motion equation:

$$\ddot{q}_i + \mu_i\dot{q}_i + \omega_i^2 q_i(t) + \sum\nolimits_{j\,=\,1}^{N} \gamma_{ij}^*\left(q_i - q_j\right) + \lambda_i q_i^3 = F(t)\delta_{i1}. \tag{33}$$

The asterisk denotes normalization by the modal mass (m_i), i.e., $\gamma_{ij}^* = \gamma_{ij}/m_i$.

Where the modal parameters are given by:

$$\begin{gathered}\mu_i = \frac{\mu_i^r}{m_i};\quad \omega_i^2 = \frac{1}{m_i}\left(E_i I_i \frac{\int_0^L \left(\phi''(x)\right)^2 dx}{\int_0^L \phi^2(x)dx} + K_{fi}\right);\\ \lambda_i = \frac{E_i A_i}{2L_i m_i}\frac{\left(\int_0^L \left(\phi'(x)\right)^2 dx\right)^2}{\int_0^L \phi^2(x)dx};\gamma_{ij}^* = \frac{\gamma_{ij}}{m_i};F(t) = \frac{P_0}{m_i\int_0^L \phi^2(x)dx}\phi(Vt).\end{gathered} \tag{34}$$

The reduced-order model obtained above corresponds to a system of coupled Duffing-type oscillators. Such nonlinear oscillators provide an efficient mathematical framework for representing the response of engineering structures exhibiting geometric or material nonlinearities under dynamic excitation. Owing to their ability to reproduce complex phenomena such as amplitude-dependent stiffness, resonance shifts, and nonlinear modal interactions, Duffing-type models have been extensively employed in nonlinear vibration analysis and structural dynamics [19]. Furthermore, when external forcing and damping are included, the dissipative terms play a fundamental role in shaping the system response, particularly through the emergence of hysteretic behaviour in the frequency–response characteristics [20].

$$\left\{\begin{array}{c}\ddot{q}_1 + \mu_1\dot{q}_1 + \omega_1^2 q_1 + \lambda_1 q_1^3 + \gamma_{12}\left(q_1 - q_2\right) = F(t)\\ \ddot{q}_2 + \mu_2\dot{q}_2 + \omega_2^2 q_2 + \lambda_2 q_2^3 + \gamma_{21}\left(q_2 - q_1\right) = 0\end{array}\right., \tag{35}$$

3.2.2. Equilibrium points and stability

- **Equilibrium points**

We seek the equilibrium points for the case N = 2, and then study the stability of the system using Equation (35). At the equilibrium, we set $\ddot{q}_1 = \dot{q}_1 = \ddot{q}_2 = \dot{q}_2 = 0,$

and $F(t) = \psi$, which gives the nonlinear algebraic system:

$$\begin{cases} \omega_1^2 q_1 + \lambda_1 q_1^3 + \gamma_{12}(q_1 - q_2) = \psi \\ \omega_2^2 q_2 + \lambda_2 q_2^3 + \gamma_{21}(q_2 - q_1) = 0 \end{cases}, \tag{36}$$

The quantity ψ denotes the static equivalent of the external excitation $F(t)$. By combining these two equations, we obtain the second equation:

$$q_1 = \frac{\left(\omega_2^2 + \gamma_{21}\right) q_2 + \lambda_2 q_2^3}{\gamma_{21}}. \tag{37}$$

$$\frac{\lambda_1 \lambda_2^3}{\gamma_{21}^3} q_2^9 + \frac{3\lambda_1\left(\omega_2^2 + \gamma_{21}\right)\lambda_2^2}{\gamma_{21}^3} q_2^7 + \frac{3\lambda_1\left(\omega_2^2 + \gamma_{21}\right)^2 \lambda_2}{\gamma_{21}^3} q_2^5 + \left(\frac{\left(\omega_1^2 + \gamma_{12}\right)\lambda_2}{\gamma_{21}} + \frac{\lambda_1\left(\omega_2^2 + \gamma_{21}\right)^3}{\gamma_{21}^3}\right) q_2^3 + \left(\frac{\left(\omega_2^2 + \gamma_{21}\right)\left(\omega_1^2 + \gamma_{12}\right)}{\gamma_{21}} - \gamma_{12}\right) q_2 - \psi = 0, \tag{38}$$

By inserting Equation (37) into Equation (36), the governing ninth-order polynomial given in Equation (38) is obtained. The equilibrium solutions are subsequently computed by varying the excitation frequency ω, and the resulting equilibrium branches are represented in the corresponding bifurcation diagrams (**Figure 2**).

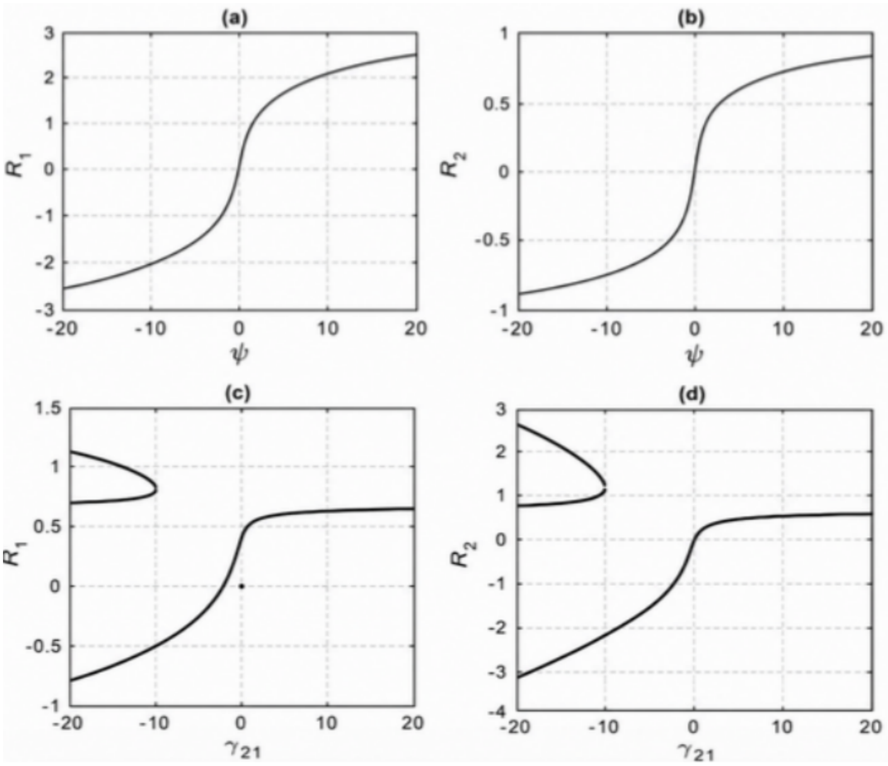

Figure 2. The equilibrium points for $\lambda_1 = 1$; $\lambda_2 = 1.5$, $\gamma_{12} = 1$, $\omega_1 = \omega_2 = 1$ and for: **(a)** and **(b)** $\gamma_{21} = 1$, and for variable *F;* **(c)** and **(d)** $\psi = 1$, and for variable γ_{21}. As can be seen, the system is sensitive to variations of γ_{21}.

- **Stability**

In order to study the stability of the above equilibrium points, let us make the change of variable $q_i = q_{0I} + \xi_i$, with $\xi_i, \ll q_{0I}$. Inserting this variable into Equation (35) and keeping only the terms of the first order of ξ_i, leads to the equation in the form

$\dot{z} = Jz$, with $z = \left[\dot{\xi}_1,\ \xi_1,\ \dot{\xi}_2,\ \xi_2\right]$, where J is the Jacobian matrix defined as

$$J = \begin{matrix} 0 & 1 & 0 & 0 \\ -\alpha_1 & -\mu_1 & \gamma_{12} & 0 \\ 0 & 0 & 0 & 1 \\ \gamma_{21} & 0 & -\alpha_2 & -\mu_2 \end{matrix}, \alpha_1 = \omega_1^2 + \gamma_{12} + 3\lambda_1 q_{01}^2, \alpha_2 = \omega_2^2 + \gamma_{21} + 3\lambda_2 q_{02}^2. \quad (39)$$

In order to find the eigenvalues of J, one can have the characteristic polynomial

$$\begin{gathered} \kappa^4 + b_1\kappa^3 + b_2\kappa^2 + b_3\kappa + b_4 = 0, \text{ with } b_1 = \mu_1 + \mu_2, \\ b_2 = \alpha_1 + \alpha_2 + \mu_1\mu_2, b_3 = \mu_1\alpha_2 + \mu_2\alpha_1, \\ b_4 = \omega_1^2\omega_2^2 + \omega_1^2\left(\gamma_{21} + 3\lambda_2 q_{02}^2\right) + \omega_2^2\left(\gamma_{12} + 3\lambda_1 q_{01}^2\right) + \\ 9\lambda_1\lambda_2 q_{01}^2 q_{02}^2 + 3\lambda_1\gamma_{21} q_{01}^2 + 3\lambda_2\gamma_{12} q_{02}^2. \end{gathered} \quad (40)$$

where κ denotes the eigenvalue of the Jacobian matrix J. According to the Routh-Hurwitz criterion, the equilibrium point (q_{01}, q_{02}) is locally asymptotically stable if all the roots of the characteristic polynomial have negative real parts. For the polynomial Equation (40), all coefficients must be positive, that is $b_1 > 0,\ b_2 > 0,\ b_3 > 0,\ b_4 > 0$. Moreover, the following criteria must be satisfied: $b_1 b_2 > b_3$, and $b_1 b_2 b_3 > b_3^2 +\ b_1^2 b_4$.

Expanding these criteria, one has:

$$\begin{gathered} \mu_1\alpha_1 + \mu_2\alpha_2 + \mu_1\mu_2(\mu_1 + \mu_2) > 0, \\ \mu_1\mu_2\left[\mu_1\alpha_2 + \mu_2\alpha_1 + \mu_1\mu_2(\alpha_1 + \alpha_2) + (\alpha_1 - \alpha_2)^2\right] + (\mu_1 + \mu_2)^2\gamma_{12}\gamma_{21} > 0. \end{gathered} \quad (41)$$

For the parameter ranges considered in this study, the above inequalities are satisfied, indicating that the corresponding equilibrium points are locally asymptotically stable. For the undamped case, that is $\mu_1 = \mu_2 = 0$, Equation (40) admits as solution $\kappa_1 = \pm i\Omega_1,\ \kappa_2 = \pm i\Omega_2$, with

$$\Omega_1 = \sqrt{\frac{\alpha_1 + \alpha_2 + \sqrt{(\alpha_1 - \alpha_2)^2 + 4\gamma_{12}\gamma_{21}}}{2}},$$

$$\Omega_2 = \sqrt{\frac{\alpha_1 + \alpha_2 - \sqrt{(\alpha_1 - \alpha_2)^2 + 4\gamma_{12}\gamma_{21}}}{2}}. \quad (42)$$

In this case, the equilibrium point (q_{01}, q_{02}) is a center point.

3.3. Analytical solutions

3.3.1. General case

Let us introduce in Equation (35) a small parameter $\varepsilon \ll 1$, such as $\mu_i = \varepsilon\mu_{i0}$, $\lambda_i = \varepsilon\lambda_{i0}$, $F = \varepsilon A_0$, $\gamma_{ij} = \varepsilon\gamma_{ij}^*$, and the variables:

$$q_i = q_{i0} + \varepsilon q_{i1} + \ldots, T_0 = t, T_1 = \varepsilon t, T_2 = \varepsilon^2 t, \ldots. \quad (43)$$

A_0 represents the harmonic amplitude of $F(t)$ used in the multiple-scale formulation. Expanding the total derivative:

$$\frac{d}{dt} = D_0 + \varepsilon D_1 + \varepsilon^2 D_2 + \ldots, D_0 = \frac{\partial}{\partial T_0}, D_1 = \frac{\partial}{\partial T_1}, D_2 = \frac{\partial}{\partial T_2}, \ldots \quad (44)$$

We obtain

- **At order zero ($\varepsilon^{\mathbf{0}}$)**

$$D_0^2 q_{i0} + \omega_i^2 q_{i0} = 0, i = 1, 2, \ldots, N \quad (45)$$

That admits fundamental solutions:

$$q_{i0} = R_i(T_1)\cos(\theta_i)\,,\ \theta_i = \omega_i T_0 - \phi_i\,(T_1) \quad (46)$$

- **Equating the coefficients associated with the first-order perturbation parameter *ε* gives**

$$\begin{gathered} D_0^2 q_{i1} + \omega_i^2 q_{i1} = A_0 \cos(\Omega T_0)\,\delta_{i1} - \sum_{j\,=\,1}^{N} \gamma_{ij}^*\,(q_{i0} - q_{j0}) \\ -\mu_{i0} D_0 q_{i0} - 2 D_0 D_1 q_{i0} - \lambda_{i0} q_{i0}^3 \end{gathered} \quad (47)$$

Thus, we obtain

$$\begin{gathered} D_0^2 q_{i1} + \omega_i^2 q_{i1} = A_0 \cos(\Omega T_0)\,\delta_{i1} - \textstyle\sum_{j\,=\,1}^{N} \gamma_{ij}^*\,(R_i \cos(\theta_i\,) - R_j \cos(\theta_j)) \\ +\,\mu_{i0}\omega_i R_i \sin(\theta_i\,) + 2\omega_i\,(D_1 R_i \sin(\theta_i\,) - R_i D_1 \phi_i \cos(\theta_i\,)) - \lambda_{i0} R_i^3 \cos^3(\theta_i). \end{gathered} \quad (48)$$

The condition for weak resonance appears when:

$$\begin{gathered} D_0^2 q_{i1} + \omega_i^2 q_{i1} = \cos(\Omega T_0)(A_0 \delta_{i1} - \sum_{j\,=\,1}^{N} \gamma_{ij}^*(R_i \cos(\psi_i) - \\ R_j \cos(\psi_j)) + (\mu_{i0}\omega_i R_i + 2\omega_i D_1 R_i)\sin(\psi_i\,) - \\ (2\omega_i R_i D_1 \phi_i + \tfrac{3}{4}\lambda_{i0} R_i^3)\cos(\psi_i\,)) \\ +\sin(\Omega T_0)(\sum_{j\,=\,1}^{N} \gamma_{ij}^*(R_i \sin(\psi_i) - R_j \sin(\psi_j)) + \\ (\mu_{i0}\omega_i R_i + 2\omega_i D_1 R_i)\cos(\psi_i) + (2\omega_i R_i D_1 \phi_i + \tfrac{3}{4}\lambda_{i0} R_i^3)\sin(\psi_i\,)) - \\ \tfrac{1}{4}\lambda_{i0} R_i^3 \cos(3\Omega T_0)\cos(3\psi_i). \end{gathered} \quad (49)$$

To prevent the occurrence of secular growth in the perturbation expansion, the coefficients of the resonant harmonics cos (ΩT_0) and sin (ΩT_0) are required to be zero. We thus obtain a system of slow differential equations for the amplitudes and phases:

$$\begin{gathered} 2\omega_i R_i D_1 \phi_i = A_0 \cos(\psi_i\,)\,\delta_{i1} - \tfrac{3}{4}\lambda_{i0} R_i^3 - \textstyle\sum_{j\,=\,1}^{N} \gamma_{ij}^*\,(R_i - R_j \cos(\psi_j - \psi_i)) \\ 2\omega_i D_1 R_i = -A_0 \sin(\psi_i\,)\,\delta_{i1} - \mu_{i0}\omega_i R_i + \textstyle\sum_{j\,=\,1}^{N} \gamma_{ij}^* R_j \sin(\psi_j - \psi_i), \\ \psi_i = \chi_i T_1 - \phi_i\,(T_1)\,, i = 1, \ldots, N. \end{gathered} \quad (50)$$

The stationary solution is obtained if and only if: $D_1 R_i = 0$, and the phase remains constant, i.e., $D_1\phi_j - D_1\phi_i = (\chi_j - \chi_i)$, and gradually, we find that the solution is $D_1\phi_i = \chi_i$.

We then obtain:

$$\begin{gathered} 2\omega_i R_i \chi_i + \tfrac{3}{4}\lambda_{i0} R_i^3 + \textstyle\sum_{j\,=\,1}^{N} \gamma_{ij}^{*}\left(R_i - R_j \cos\left(\psi_{ij}\right)\right) = A_0 \cos\left(\psi_i\ \right)\delta_{i1}, \\ \sum_{j\,=\,1}^{N} \gamma_{ij}^{*} R_j \sin\left(\psi_{ij}\right) - \mu_{i0}\omega_i R_i = A_0 \sin\left(\psi_i\ \right)\delta_{i1},\ \psi_{ij}, = \psi_i - \psi_j,\ i = 1, \ldots, N. \end{gathered} \tag{51}$$

This leads to a system of equations that can be solved to find the amplitudes at different rail levels.

3.3.2. For the particular case where N = 2

We get:

$$\begin{cases} -\omega_1\mu_{10}R_1 + \gamma_{12}^{*}R_2\sin\left(\psi_{12}\right) = A_0\sin\left(\psi_1\right) \\ \left(2\omega_1\chi_1 + \gamma_{12}^{*}\right)R_1 + \frac{3}{4}\lambda_{10}R_1^3 - \gamma_{12}R_2\cos\left(\psi_{12}\right) = A_0\cos\left(\psi_1\right) \\ \omega_2\mu_{20}R_2 + \gamma_{21}^{*}R_1\sin\left(\psi_{12}\right) = 0, \\ \left(2\omega_2\chi_2 + \gamma_{21}^{*}\right)R_2 + \frac{3}{4}\lambda_{20}R_2^3 - \gamma_{21}^{*}R_1\cos\left(\psi_{12}\right) = 0. \end{cases} \tag{52}$$

By eliminating the trigonometric angles from the last two lines of Equation (52), we obtain:

$$\begin{gathered} R_1 = \frac{R_2}{\gamma_{21}^{*}}\sqrt{\omega_2^2\mu_{20}^2 + \left(2\omega_2\chi_2 + \gamma_{21}^{*} + \frac{3}{4}\lambda_{20}R_2^2\right)^2}, \\ \tan\left(\psi_{12}\right) = \frac{-\omega_2\mu_{20}}{2\omega_2\chi_2 + \gamma_{21}^{*} + \frac{3}{4}\lambda_{20}R_2^2}. \end{gathered} \tag{53}$$

By combining the first two lines of Equation (52), we obtain:

$$\begin{gathered} A_0^2\,\gamma_{21}^{*2}R_1^2 \ = \left(\gamma_{21}^{*}\omega_1\mu_{10}R_1^2 + \gamma_{12}^{*}\omega_2\mu_{20}R_2^2\right)^2 \\ + \left(\gamma_{21}^{*}\left(2\omega_1\chi_1 + \gamma_{12}^{*}\right)\ R_1^2 + \frac{3}{4}\gamma_{21}^{*}\lambda_{10}R_1^4 \ \ -\gamma_{12}^{*}R_2^2\left(2\omega_2\chi_2 + \gamma_{21}^{*} + \frac{3}{4}\lambda_{20}R_2^2\right)\right)^2\ , \end{gathered} \tag{54}$$

where: $\omega_i = \Omega + \varepsilon\chi_i$. Equation (54) can be transformed into a polynomial equation of degree 24 with respect to the modal amplitude. Owing to its cumbersome analytical form, the polynomial is solved numerically.

Figure 3 presents the frequency-response curves of the vibration amplitudes R_1 and R_2, corresponding respectively to the first and second beam layers, over the frequency range ($0 \leq \Omega \leq 5$), $\Omega = \omega_1 - \chi_1 = \omega_2 - \chi_2$. The results are shown for two excitation amplitudes, ($A_0 = 1$, black curves) and ($A_0 = 1.5$, red curves). The coexistence of several solution branches reveals a pronounced nonlinear behaviour and the presence of multistable responses.

For the first beam layer (R_1, **Figure 3a**,**b**), the response exhibits a marked resonance region centred around ($\Omega \ \approx\ 2$). Increasing the excitation amplitude from ($A_0 = 1$) to ($A_0 = 1.5$) substantially increases the vibration amplitude and enlarges the interval where multiple steady-state solutions coexist. The bending of the response curves and the appearance of disconnected branches indicate nonlinear hardening effects and branch-jump phenomena.

The second beam layer (R_2, **Figure 3c**,**d**) displays a similar nonlinear frequency response, although with lower amplitudes than those observed in the first layer.

Resonance occurs approximately within the interval ($1.5 \leq \Omega \leq 2.5$), where multiple solution branches are also observed. As the excitation amplitude increases, the vibration level rises and the hysteretic behaviour becomes more pronounced. Overall, **Figure 3** demonstrates that the excitation amplitude strongly influences the dynamic response of both beam layers. Higher forcing levels enhance the resonance amplitudes, enlarge the multistability regions, and promote branch-jump phenomena. These results highlight the significant role of nonlinear interlayer coupling in shaping the frequency-response characteristics of the proposed beam model.

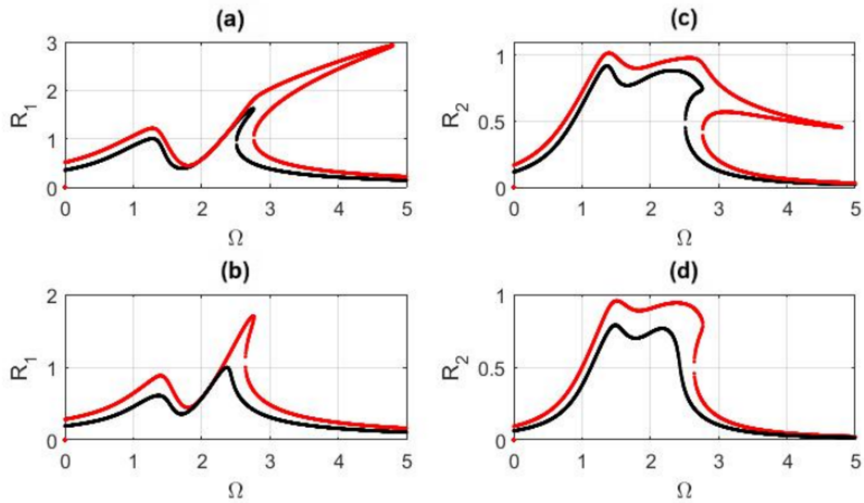

Figure 3. Frequency–amplitude response predicted by the proposed nonlinear model as a function of the detuning parameter Ω, with $\Omega = \omega_1 - \chi_1 = \omega_2 - \chi_2$.
Note: The results are obtained for $\omega_2 = 1$, $\gamma_{12} = \gamma_{21} = 1$, $\lambda_{10} = \lambda_{20} = 1$, $\mu_{10} = \mu_{20} = 0.5$. The black curves correspond to: $A_0 = 1$, whereas the red curves represent: $A_0 = 1.5$. Curves (a, c) and (b,d) illustrate the cases $\omega_1 = 1$, and $\omega_1 = 1.5$, respectively.

3.3.3. For the particular case where N = 3

We obtain a very complex system, where initially, we neglect the terms involving higher-order neighbours. This gives us:

$$\begin{gathered}
R_2 = \tfrac{R_3}{\gamma_{23}^*}\sqrt{\left(\gamma_{23}^* + 2\omega_3\chi_3 + \tfrac{3}{4}\lambda_{30}R_3^2\right)^2 + \left(\mu_{30}\omega_3\right)^2}, \\
\tan\left(\psi_{23}\right) = -\frac{\mu_{30}\omega_3}{\gamma_{23}^* + 2\omega_3\chi_3 + \frac{3}{4}\lambda_{30}R_3^2}, \\
R_1 = \tfrac{1}{\gamma_{21}^* R_2}\sqrt{A^2 + \left(\mu_{30}\omega_3R_3^2 + \mu_{20}\omega_2R_2^2\right)^2}\,, \\
A = \left(\gamma_{21}^* + \gamma 23^* + 2\omega_2\chi_2 + \tfrac{3}{4}\lambda_{20}R_2^2\right)R_2^2 - \left(\gamma_{23}^* + 2\omega_3\chi_3 + \tfrac{3}{4}\lambda_{30}R_3^2\right)R_3^2, \\
\tan\left(\psi_{21}\right) = -\frac{\mu_{20}\omega_2R_2^2 + \mu_{30}\omega_3R_3^2}{A},
\end{gathered} \tag{55}$$

$$\begin{gathered}
T_2 = \gamma_{21}^* + \gamma_{23}^* + 2\omega_2\chi_2 + \tfrac{3}{4}\lambda_{20}R_2^2, T_1 = \gamma_{12}^* + 2\omega_1\chi_1 + \tfrac{3}{4}\lambda_{10}R_1^2, \\
T_3 = \gamma_{32}^* + 2\omega_3\chi_3 + \tfrac{3}{4}\lambda_{30}R_3^2, \\
A_0^2\left(A^2 + \left(\mu_{30}\omega_3R_3^2 + \mu_{20}\omega_2R_2^2\right)^2\right)R_2^2 \\
= {\gamma_{21}^*}^2R_2^2[\left(\mu_{20}\,\omega_2\,R_2^4 + \mu_{30}\,\omega_3R_3^2R_2^2\; + \mu_{10}\,\omega_1\,R_1^2\,R_2^2\,\right)^2 \\
+ \left(T_1R_1^2R_2^2\; + T_2R_2^4 + T_3R_3^2R_2^2\right)^2].
\end{gathered} \tag{56}$$

Equation (56) was solved numerically, and the resulting frequency-response curves are presented in **Figure 4** for the three-layer beam system N = 3. The amplitudes R_1, R_2, and R_3, corresponding to the three beam layers, exhibit strongly nonlinear behaviour over the frequency range $1 \leq \omega \leq 3$. Unlike the two-layer configuration, the addition of a third layer considerably increases the complexity of the response, leading to the coexistence of multiple solution branches and extended hysteretic regions. Depending on the excitation frequency, the system may admit two, three, or four steady-state solutions, indicating pronounced multistability.

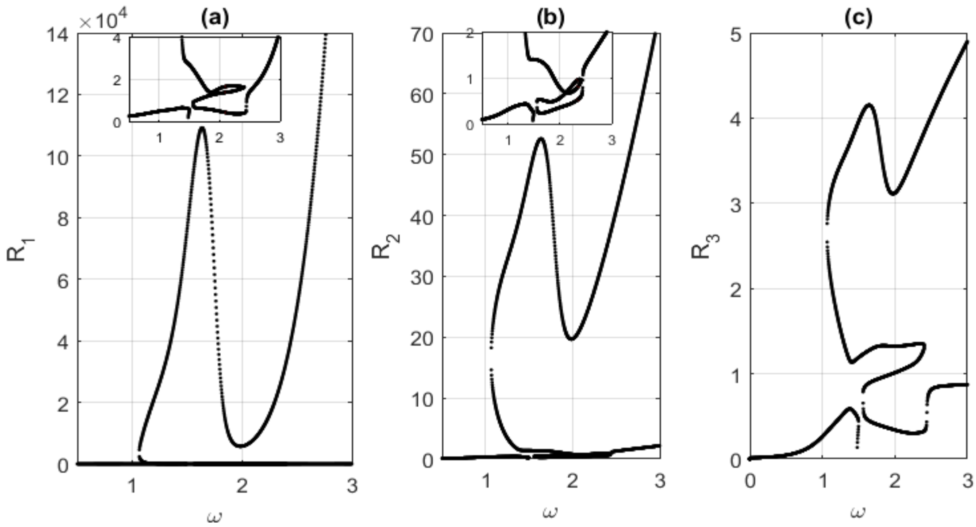

Figure 4. Frequency–amplitude response predicted by the proposed nonlinear model as a function of the detuning parameter Ω for N = 3, with and for $\omega_1 = \omega_2 = \omega_3 = 1$, $\gamma_{12} = \gamma_{21} = \gamma_{23} = \gamma_{32} = 1$, $\lambda_{10} = \lambda_{20} = \lambda_{30} = 1$, $\mu_{10} = \mu_{20} = \mu_{30} = 0.5$, $A_0 = 1$.

The response of the first layer is characterized by larger vibration amplitudes, whereas the second and third layers exhibit more complex branch structures resulting from the transfer and redistribution of energy through the interlayer coupling. The folds and disconnected branches observed in the frequency-response curves are typical signatures of saddle-node bifurcations, giving rise to branch-jump phenomena and abrupt changes in vibration amplitude. These results demonstrate that nonlinear coupling not only modifies the resonance characteristics of each layer but also enhances the sensitivity of the system to frequency variations. Consequently, the three-layer beam system exhibits richer nonlinear dynamics, with strong multistability and complex resonance patterns that are absent or less pronounced in the two-layer configuration.

4. Numerical simulation results

Numerical simulations were performed for two distinct cases involving geometric and material configurations. The variables studied were the displacements and the dominant degrees of freedom associated with them. For each configuration, the temporal responses, phase portraits, and Fourier spectra were extracted. In all simulations, we assume: $F_1(t) = A_0 \cos(\omega t)$.

4.1. Case N = 2

4.1.1. Effect of the excitation frequency ω

Figure 5 presents the temporal responses, phase portraits, and frequency spectra of the two-layer beam system N = 2 for $\omega_1 = 1.2$, $\omega_2 = 1$, $\lambda_1 = 0.25$, $\lambda_2 = 1$, $\mu_1 = \mu_2 = 7.5 \times 10^{-5}$, $A_0 = 5 \times 10^{-3}$ and $\omega = 1.8$. The displacement histories $q_1(t)$ and $q_2(t)$ exhibit bounded oscillations with nearly constant amplitudes, indicating a stable dynamic regime. This behaviour is corroborated by the phase portraits, which form closed trajectories characteristic of periodic motion and the absence of dynamic instability.

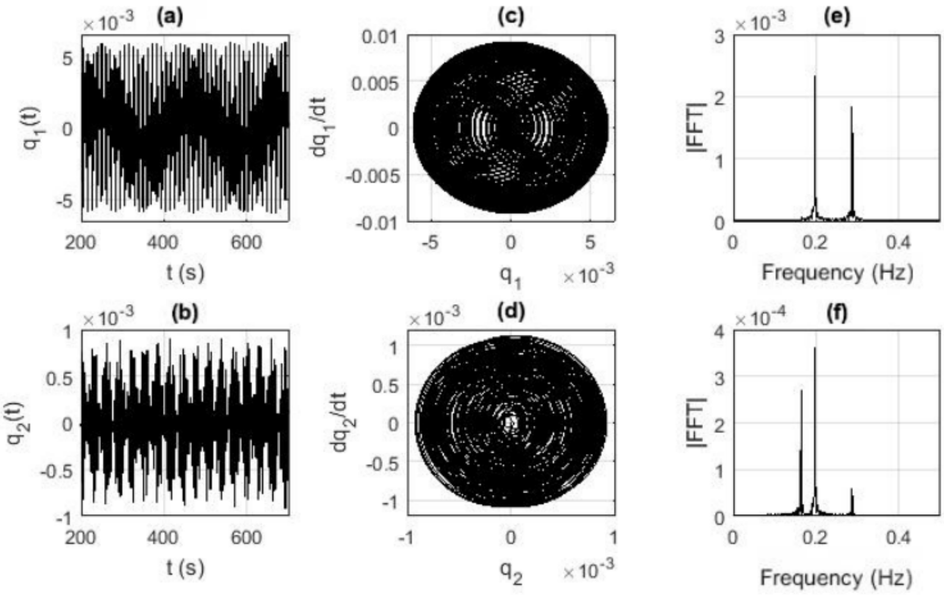

Figure 5. Dynamic response of the two-layer beam configuration (N = 2): **(a)** and **(b)** time history of the transverse displacement; **(c)** and **(d)** corresponding phase trajectory; **(e)** and **(f)** Fourier amplitude spectrum computed for the following parameter values: $\omega_1 = 1.2$, $\omega_2 = 1$, $\lambda_1 = 0.25$, $\lambda_2 = 1$, $\mu_1 = \mu_2 = 7.5 \times 10^{-5}$, $A_0 = 5 \times 10^{-3}$ and $\omega = 1.8$.

The corresponding frequency spectra are dominated by a limited number of well-defined peaks concentrated around the fundamental vibration frequencies, showing that the response is governed by a small set of interacting modes. The absence of significant broadband components suggests that the motion remains regular, without chaotic behaviour or strong nonlinear modal interactions. Overall, the combined time-domain, phase-space, and spectral analyses indicate that the system operates in a stable periodic regime under the selected excitation conditions, with vibration energy mainly concentrated in the dominant response frequencies.

Figure 6 presents the dynamic response of the two-layer beam system for the same set of parameters as in **Figure 5**, with the addition of the interlayer coupling coefficients $\gamma_{12} = \gamma_{21} = 7 \times 10^{-2}$. Compared with the uncoupled case, the introduction of coupling modifies the vibration patterns of both layers through energy exchange mechanisms between them. This effect is reflected in the increased modulation of the displacement histories and the more intricate structures observed in the phase portraits. The frequency spectra reveal the appearance of additional spectral components associated with the coupling-induced interactions between the two layers. Although the dominant frequencies remain close to the fundamental vibration frequencies of the system, the response becomes richer due to the transfer of energy between the coupled layers. These results demonstrate that the interlayer coupling plays a significant role in shaping the dynamic behaviour of the structure by promoting modal interactions and altering the distribution of vibration energy throughout the system.

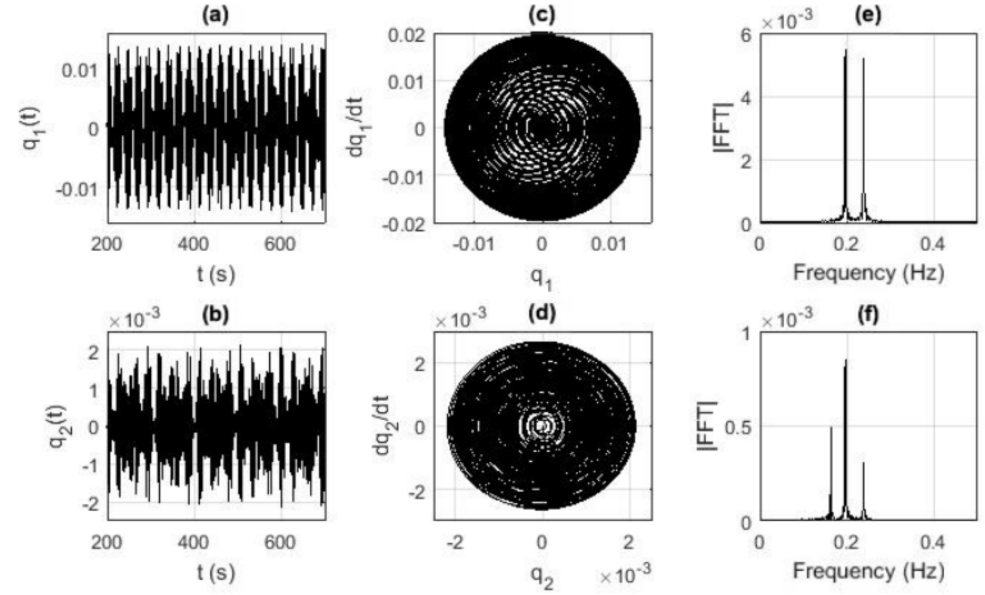

Figure 6. Dynamic response of the two-layer beam configuration (N = 2): **(a)** and **(b)** time history of the transverse displacement; **(c)** and **(d)** corresponding phase trajectory; **(e)** and **(f)** Fourier amplitude spectrum computed for the following parameter values: $\omega_1 = 1.2$, $\omega_2 = 1$, $\gamma_{21} = \gamma_{12} = 7 \times 10^{-2}$, $\lambda_1 = 0.25$, $\lambda_2 = 1$, $\mu_1 = \mu_2 = 7.5 \times 10^{-5}$, $A_0 = 5 \times 10^{-3}$ and ω = 1.5.

Figure 7 presents the dynamic response of the two-layer beam system under the same conditions as in **Figure 6**, except for the excitation frequency, which is reduced to ($\omega = 0.02$). This modification significantly alters the system dynamics, leading to the emergence of a quasi-periodic response. The displacement histories exhibit pronounced amplitude modulations and beating phenomena, indicating the coexistence of several interacting frequencies. This transition is further reflected in the phase portraits, whose trajectories no longer collapse onto simple closed orbits but instead occupy a broader region of the phase space. The frequency spectra confirm the multi-frequency nature of the response through the appearance of additional spectral components around the dominant frequencies. These results reveal enhanced energy exchanges between the coupled layers and demonstrate that lowering the excitation frequency promotes quasi-periodic oscillations driven by nonlinear modal interactions.

Figure 8 presents the dynamic response of the two-layer beam system for the same excitation conditions as in **Figure 7**, but with identical natural frequencies ($\omega_1 = \omega_2 = 0.05$). This modal matching significantly modifies the system dynamics by strengthening the interaction between the two coupled layers. The temporal responses exhibit larger amplitude fluctuations and more pronounced modulation patterns, indicating an enhanced exchange of energy between.

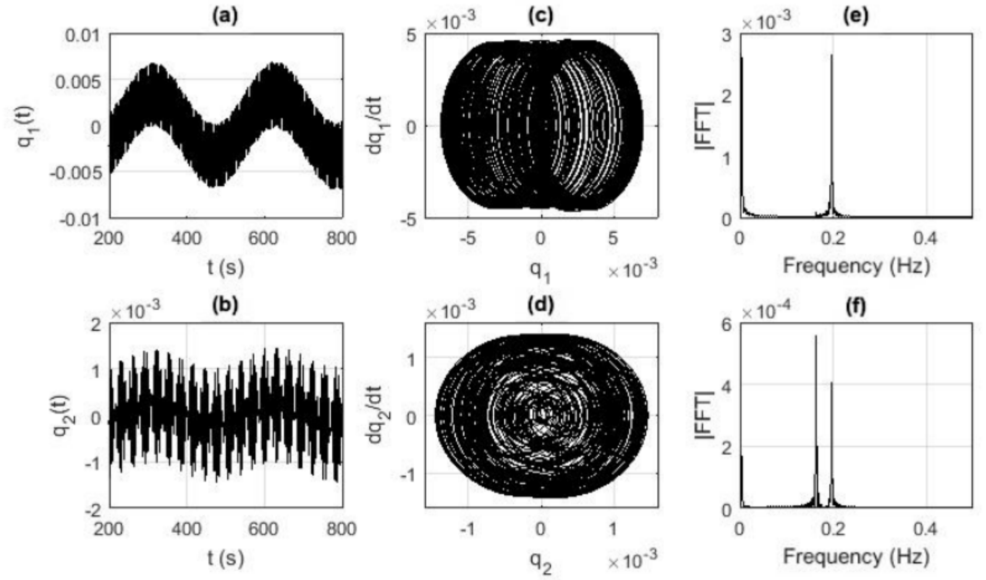

Figure 7. Dynamic response of the two-layer beam configuration (N = 2): **(a)** and **(b)** time history of the transverse displacement; **(c)** and **(d)** corresponding phase trajectory; **(e)** and **(f)** Fourier amplitude spectrum computed for the following parameter values: $\omega_1 = 1.2$, $\omega_2 = 1$, $\gamma_{21} = \gamma_{12} = 7 \times 10^{-2}$, $\lambda_1 = 0.25$, $\lambda_2 = 1$, $\mu_1 = \mu_2 = 7.5 \times 10^{-5}$, $A_0 = 5 \times 10^{-3}$ and $\omega = 0.02$.

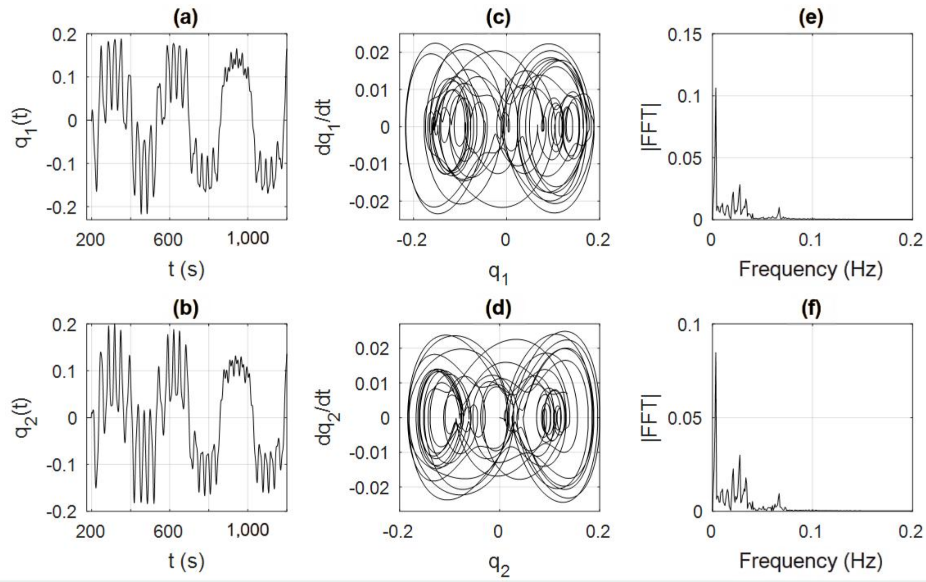

Figure 8. Dynamic response of the two-layer beam configuration (N = 2): **(a)** and **(b)** time history of the transverse displacement; **(c)** and **(d)** corresponding phase trajectory; **(e)** and **(f)** Fourier amplitude spectrum computed for the following parameter values: $\omega_1 = \omega_2 = 0.05$, $\gamma_{21} = \gamma_{12} = 7 \times 10^{-2}$, $\lambda_1 = 0.25$, $\lambda_2 = 1$, $\mu_1 = \mu_2 = 7.5 \times 10^{-5}$, $A_0 = 5 \times 10^{-3}$, and $\omega = 0.02$.

Figure 9 presents the dynamic response of the two-layer beam system for the same parameters as in **Figure 8**, except that the excitation frequency is increased to $\omega = 0.2$. This change modifies the energy distribution within the structure and leads to larger vibration amplitudes in both beam layers. The temporal responses remain bounded but exhibit more pronounced oscillations, indicating a stronger contribution of the external excitation to the system dynamics.

The phase portraits remain confined within finite regions of the phase space, confirming that the response preserves its overall stability despite the increase in vibration level. Compared with the previous case, the trajectories become larger and more distorted, reflecting enhanced nonlinear interactions between the coupled layers. The corresponding frequency spectra show a broader distribution of spectral components around the dominant frequencies, revealing stronger modal interactions and a more significant contribution of higher-order harmonics.

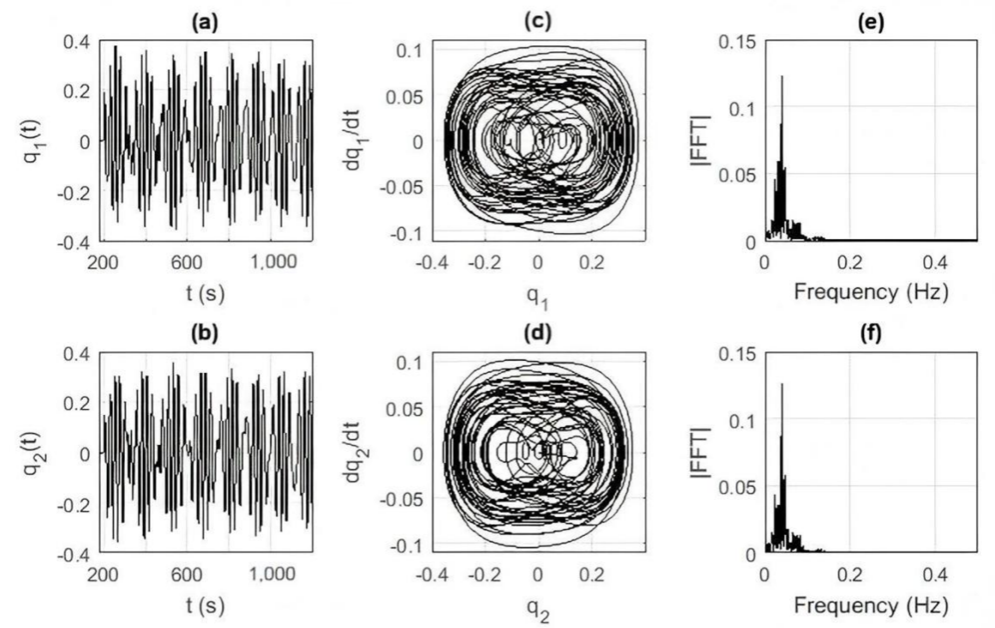

Figure 9. Dynamic response of the two-layer beam configuration (N = 2): **(a)** and **(b)** time history of the transverse displacement; **(c)** and **(d)** corresponding phase trajectory; **(e)** and **(f)** Fourier amplitude spectrum computed for the following parameter values: $\omega_1 = \omega_2 = 0.05$, $\gamma_{21} = \gamma_{12} = 7 \times 10^{-2}$, $\lambda_1 = 0.25$, $\lambda_2 = 1$, $\mu_1 = \mu_2 = 7.5 \times 10^{-5}$, $A_0 = 5 \times 10^{-3}$ and $\omega = 0.2$.

Overall, **Figure 9** demonstrates that increasing the excitation frequency intensifies the dynamic response and promotes nonlinear energy exchanges between the two layers. Although the vibration amplitudes and spectral richness increase, the system remains in a bounded oscillatory regime, indicating that the nonlinear interactions modify the response characteristics without inducing a loss of stability.

4.1.2. Effect of the input amplitude A_0

Figure 10 illustrates the dynamic response of the two-layer beam system for the same parameters as in **Figure 9**, but with a significantly larger excitation amplitude $A_0 = 0.25$. The increase in forcing intensity substantially amplifies the vibration levels of both layers and enhances the influence of nonlinear effects on the system dynamics. The displacement histories exhibit larger oscillation amplitudes together with pronounced modulation patterns, indicating stronger energy exchanges between the coupled layers. The phase portraits expand considerably compared with the previous cases and display more distorted trajectories, revealing the growing contribution of nonlinear interactions. However, the trajectories remain bounded, indicating that the response preserves its overall stability despite the stronger excitation.

The corresponding frequency spectra show a richer harmonic content, with additional spectral components generated by nonlinear modal coupling and energy redistribution mechanisms.

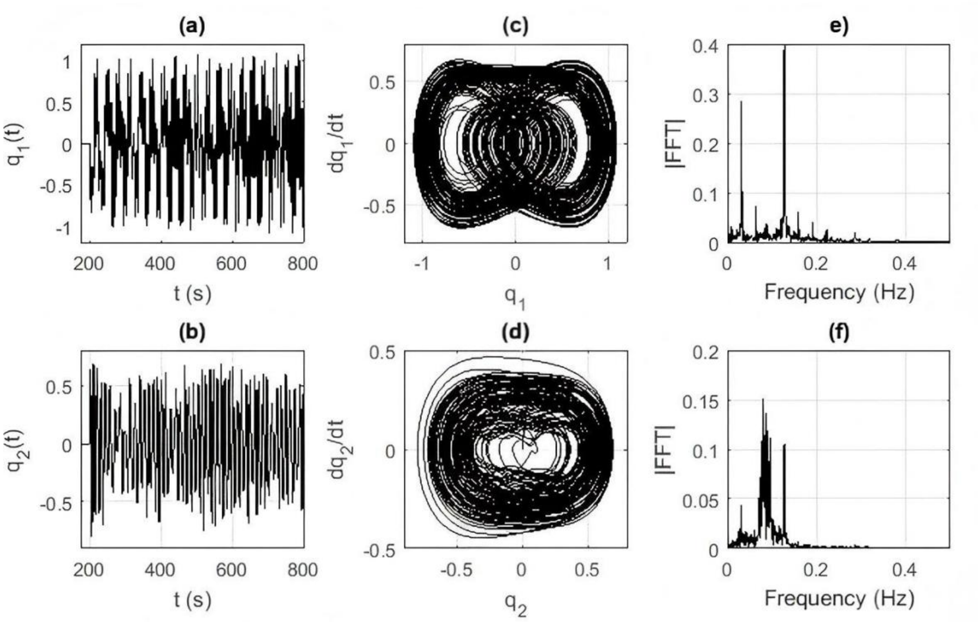

Figure 10. Dynamic response of the two-layer beam configuration (N = 2): **(a)** and **(b)** time history of the transverse displacement; **(c)** and **(d)** corresponding phase trajectory; **(e)** and **(f)** Fourier amplitude spectrum computed for the following parameter values: $\omega_1 = \omega_2 = 0.05$, $\gamma_{21} = \gamma_{12} = 7 \times 10^{-2}$, $\lambda_1 = 0.25$, $\lambda_2 = 1$, $\mu_1 = \mu_2 = 7.5 \times 10^{-5}$, $A_0 = 0.25$ and $\omega = 0.2$.

Overall, **Figure 10** demonstrates that the excitation amplitude is a key parameter governing the vibration intensity of the multilayer beam system. Increasing A_0 strengthens modal interactions, broadens the spectral content, and amplifies the response amplitudes, while the system remains in a bounded nonlinear oscillatory regime. These results highlight the important role of excitation intensity in the development of complex nonlinear vibration patterns in coupled multilayer structures.

Figure 11 extends the observations of **Figure 10** by considering a higher excitation amplitude $A_0 = 0.75$. Under this stronger forcing, the system undergoes a qualitative change in its dynamic response. The temporal signals exhibit pronounced envelope variations, indicating intensified energy exchanges between the coupled layers and a stronger sensitivity to nonlinear interactions. The phase portraits reveal increasingly intricate trajectories that no longer resemble the regular oscillatory patterns observed at lower excitation levels. This evolution reflects the growing influence of nonlinear mechanisms, which alter the structure of the attractor and promote more complex motions in the phase space. The frequency spectra show the emergence of numerous secondary components and combination frequencies, indicating that energy is redistributed over a wider frequency range. Such behaviour is characteristic of strong nonlinear modal interactions, where the response can no longer be described solely by the dominant vibration frequencies.

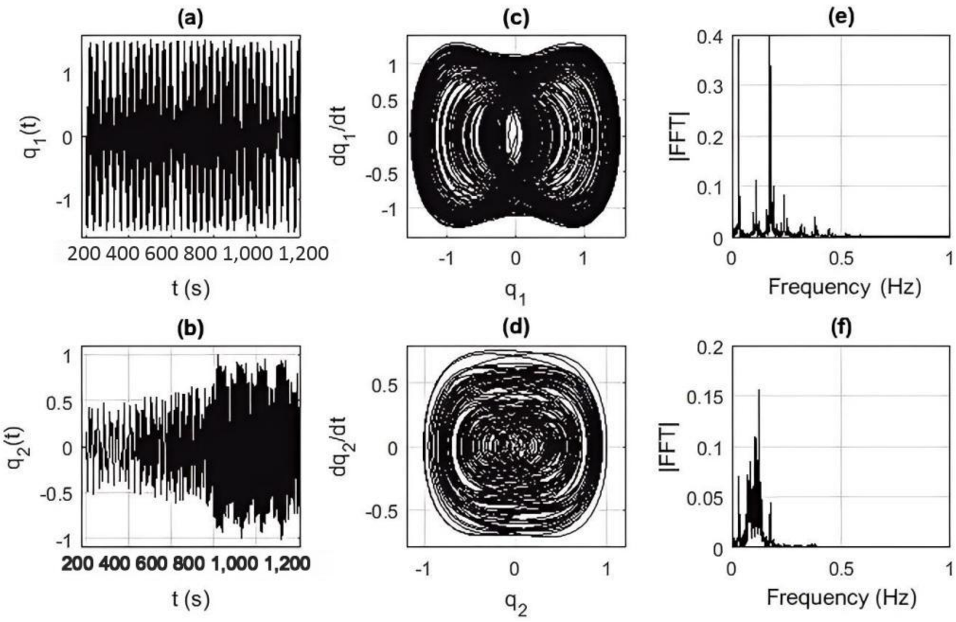

Figure 11. Dynamic response of the two-layer beam configuration (N = 2): **(a)** and **(b)** time history of the transverse displacement; **(c)** and **(d)** corresponding phase trajectory; **(e)** and **(f)** Fourier amplitude spectrum computed for the following parameter values: $\omega_1 = \omega_2 = 0.05$, $\gamma_{21} = \gamma_{12} = 7 \times 10^{-2}$, $\lambda_1 = 0.25$, $\lambda_2 = 1$, $\mu_1 = \mu_2 = 7.5 \times 10^{-5}$, $A_0 = 0.75$ and $\omega = 0.2$.

Overall, **Figure 11** highlights the transition from a moderately nonlinear regime to a strongly nonlinear oscillatory state. The increased excitation level promotes substantial modal coupling and frequency mixing, demonstrating the important role of forcing amplitude in shaping the complex dynamics of multilayer beam systems.

4.2. Case N = 3

Figure 12 presents the dynamic response of the three-layer beam system (N = 3) for $\omega_1 = \omega_2 = \omega_3 = 0.05$, $\gamma_{21} = \gamma_{12} = 7 \times 10^{-3}$, $\gamma_{23} = \gamma_{32} = 6 \times 10^{-3}$, $\gamma_{31} = \gamma_{13} = 0$, $\lambda_1 = \lambda_2 = \lambda_3 = 1$, $\mu_1 = \mu_2 = \mu_3 = 7.5 \times 10^{-5}$, $A_0 = 5 \times 10^{-3}$ and $\omega = 0.2$. Compared with the two-layer configurations analysed previously, the introduction of a third coupled layer increases the number of interacting vibration modes and consequently enriches the overall dynamics of the structure. The vibration energy is redistributed among the three beam layers, leading to more complex modal interactions and a richer spectral content. The intermediate layer plays a key role in transmitting energy between the upper and lower layers, since the direct coupling terms γ_{13} and γ_{31} are absent. As a result, the three layers exhibit distinct dynamic responses despite having identical natural frequencies. The phase portraits remain bounded, indicating that the motion is stable, while the frequency spectra reveal the contribution of several interacting modes associated with the multilayer configuration.

Overall, **Figure 12** shows that increasing the number of layers fundamentally alters the energy-transfer mechanisms within the structure. The additional degree of freedom promotes stronger modal interactions and a more complex vibration response than that observed for the two-layer beam system.

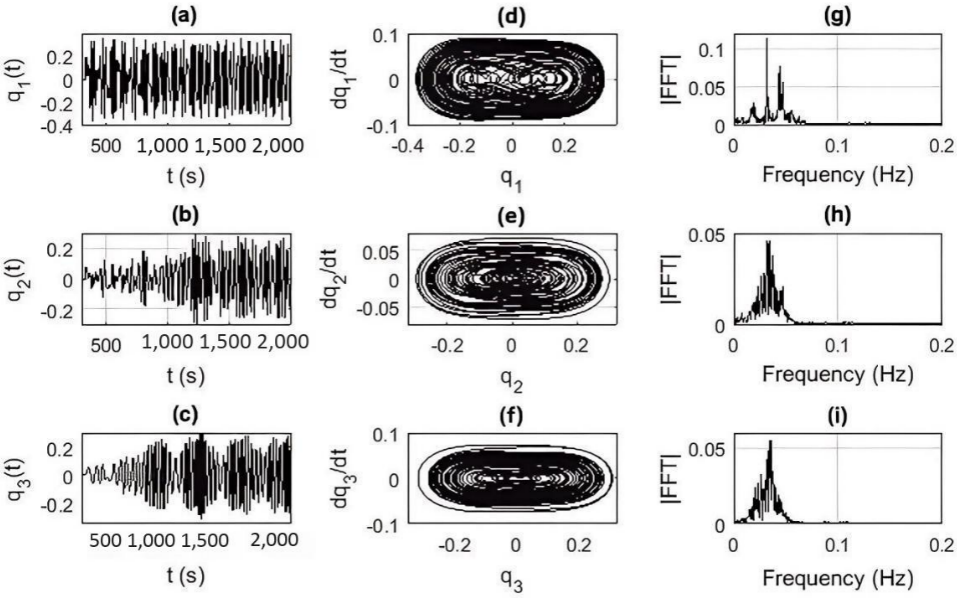

Figure 12. Dynamic response of the three-layer beam configuration (N = 3): **(a)**, **(b)**, and **(c)** time history of the transverse displacement; **(d)**, **(e)**, and **(f)** corresponding phase trajectory; **(g)**, **(h)**, and **(i)** Fourier amplitude spectrum computed for the following parameter values: $\omega_1 = \omega_2 = \omega_3 = 0.05$, $\gamma_{21} = \gamma_{12} = 7 \times 10^{-3}$, $\gamma_{23} = \gamma_{32} = 6 \times 10^{-3}$, $\gamma_{31} = \gamma_{13} = 0$, $\lambda_1 = \lambda_2 = \lambda_3 = 1$, $\mu_1 = \mu_2 = \mu_3 = 7.5 \times 10^{-5}$, $A_0 = 5 \times 10^{-3}$ and $\omega = 0.2$.

Figure 13 highlights the influence of a reduced excitation frequency $\omega = 0.02$ on the dynamic response of the three-layer beam system. In contrast to **Figure 12**, the lower forcing frequency induces a clear modulation of the vibration amplitudes, leading to beating phenomena in the displacement histories. This behaviour indicates that the external excitation interacts with the intrinsic oscillatory mechanisms of the structure over longer time scales.

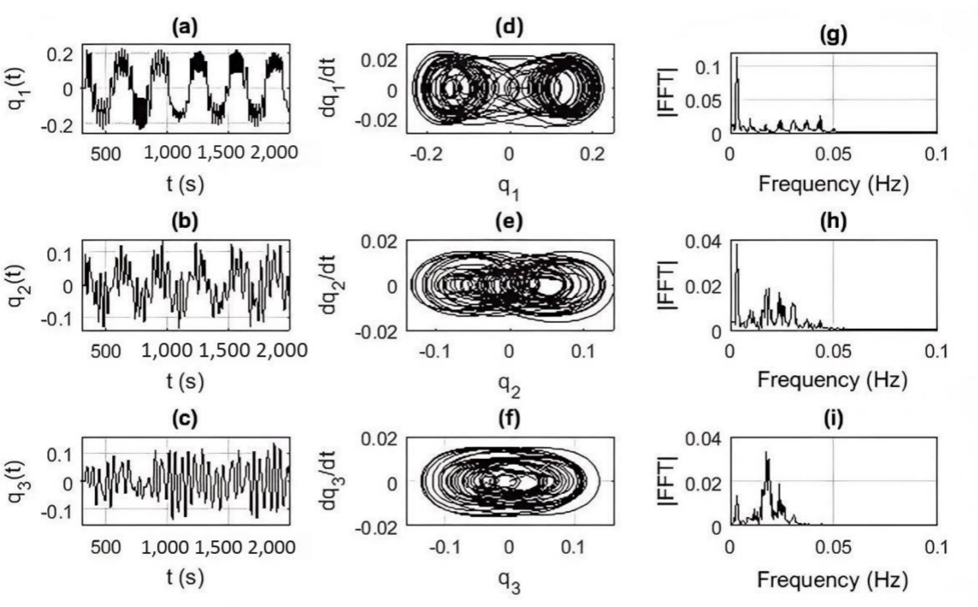

Figure 13. Dynamic response of the three-layer beam configuration (N = 3): **(a)**, **(b)**, and **(c)** time history of the transverse displacement; **(d)**, **(e)**, and **(f)** corresponding phase trajectory; **(g)**, **(h)**, and **(i)** Fourier amplitude spectrum computed for the following parameter values: $\omega_1 = \omega_2 = \omega_3 = 0.05$, $\gamma_{21} = \gamma_{12} = 7 \times 10^{-3}$, $\gamma_{23} = \gamma_{32} = 6 \times 10^{-3}$, $\gamma_{31} = \gamma_{13} = 0$, $\lambda_1 = \lambda_2 = \lambda_3 = 1$, $\mu_1 = \mu_2 = \mu_3 = 7.5 \times 10^{-5}$, $A_0 = 5 \times 10^{-3}$ and $\omega = 0.02$.

The phase portraits become less compact and exhibit trajectories that no longer follow a simple repetitive pattern. This evolution reflects the coexistence of several characteristic frequencies contributing simultaneously to the response. Consequently, the motion departs from a purely periodic regime and evolves toward a quasi-periodic state.

The spectral analysis supports this observation through the appearance of additional low-frequency components surrounding the dominant peaks. These spectral contributions reveal the emergence of slow modulation frequencies generated by the interaction between the excitation and the natural dynamics of the structure.

Overall, **Figure 13** shows that lowering the excitation frequency does not significantly increase the vibration amplitudes, but fundamentally changes the nature of the response. The system evolves from a predominantly periodic oscillation to a quasi-periodic regime characterized by amplitude modulation and multi-frequency behaviour.

4.3. Controller study

The control of vibrations in the multilayer beam is studied using a delayed controller, applied to all degrees of freedom. The basic equation of the system is provided in the previous section Equation (33). The development below shows the linearization and matrix formulation for the stability study with delayed control.

4.3.1. Principle of delayed control

The delayed controller is applied to all degrees of freedom and is defined for each modal coordinate as:

$$u_i(t) = -K\left(q_i(t) - q_i(t-\tau)\right). \tag{57}$$

Where $K > 0$ is the feedback gain and $\tau > 0$ is the delay applied. The control input is applied to each degree of freedom of the multilayer beam system.

4.3.2. Linearization and stability analysis of the delayed-controlled system

By neglecting the nonlinear terms, we obtain the linearized system for

$$q(t) = \begin{bmatrix} q_1(t) \\ q_2(t) \\ \vdots \\ q_N(t) \end{bmatrix}, \Gamma = \begin{bmatrix} \sum_{\substack{j=1 \\ j \neq 1}}^{N} \gamma_{1j} & -\gamma_{12} & \cdots & -\gamma_{1N} \\ -\gamma_{21} & \sum_{\substack{j=1 \\ j \neq 2}}^{N} \gamma_{2j} & \cdots & -\gamma_{2N} \\ \vdots & \vdots & \ddots & \vdots \\ -\gamma_{N1} & -\gamma_{N2} & \cdots & \sum_{\substack{j=1 \\ j \neq N}}^{N} \gamma_{Nj} \end{bmatrix}, F(t) = \begin{bmatrix} F(t) \\ 0 \\ \vdots \\ 0 \end{bmatrix} \tag{58}$$

$$\ddot{q}(t) + \mu\dot{q}(t) + \left(\Omega^2 + KI\right)q(t) + \Gamma q(t) - KIq(t-\tau) = F(t) \tag{59}$$

where: $\Omega^2 = diag\left(\omega_1^2, ..., \omega_N^2\right)$, $\mu = diag\left(\mu_1, ..., \mu_N\right)$. We seek the homogeneous solution of the form $q(t) = Q\exp(st)$ which leads to the matrix equation:

$$BQ = 0,\ B = s^2I + s\mu + \Omega^2 + \Gamma + K\left(1 - e^{-s\tau}\right)I. \tag{60}$$

The stability condition is obtained from the non-trivial solution requirement $\det[B(s)] = 0$. The stability analysis of delayed systems is classically performed through the roots of the transcendental characteristic equation, whose spectrum determines the asymptotic behaviour of the system. By setting $\gamma_{ij} = \gamma_{ji}$, the matrix $A = \Omega^2 + \Gamma$ is symmetric, and it admits a complete set of eigenvalues λ_i and corresponding eigenvectors ϕ_i, satisfying $A\phi_i = \lambda_i\phi_i$. For a particular case where N = 2, one has

$$\lambda_{1,2} = \frac{\omega_1^2 + \omega_2^2 + 2\gamma_{12}}{2} \pm \sqrt{\left(\omega_1^2 - \omega_2^2\right)^2 + 4\gamma_{12}^2}. \tag{61}$$

Since the matrix $\Omega^2+\Gamma$ is symmetric, the modal decomposition allows the delayed system to be expressed as a set of independent scalar delay differential equations, whose stability can be studied through their characteristic roots [21].

$$s^2 + s\mu_i + \lambda_i + K\left(1 - e^{-s\tau}\right) = 0,\ i = 1,\ 2,\ \ldots, N. \tag{62}$$

Where μ_i represents the modal damping coefficient associated with the *i*-th mode. To determine the stability boundaries, the critical roots are assumed to lie on the imaginary axis, namely $s = i\omega$. Following the frequency-domain approach commonly used in time-delay systems, the stability boundaries are determined by locating purely imaginary characteristic roots. Substituting this expression into the characteristic equation and separating the resulting equation into real and imaginary parts leads Equation (62) to

$$-\omega^2 + \lambda_i + K\left(1 - \cos(\omega\tau)\right) = 0, \mu_i\omega + K sin(\omega\tau) = 0. \tag{63}$$

The simultaneous solution of the real and imaginary parts provides the critical frequencies and the corresponding delay values at which characteristic roots cross the imaginary axis, indicating a possible stability switch and Hopf bifurcation. Solving this coupled set of equations leads to the following characteristic equation:

$$\omega^4 + \left(\mu_i^2 - 2\lambda_i - 2K\right)\omega^2 + \lambda_i^2 + 2K\lambda_i = 0. \tag{64}$$

The positive solutions of Equation (64) define the critical frequencies ω_c at which the characteristic roots cross the imaginary axis. The corresponding critical delay values are obtained from Equation (63) as

$$\tau_{cim} = \frac{1}{\omega_c}\left(2m\pi + \text{atan2}\left(-\frac{\mu_i\omega_c}{K}, 1 + \frac{\lambda_i - \omega_c^2}{K}\right)\right),\ m = 0,\ 1,\ 2, \cdots. \tag{65}$$

The quantity $\tau_{\max} = \min\left(\tau_{cim} > 0\right)$ represents the delay margin of the closed-loop system and defines the stability boundary in the (K,τ) parameter space. The delayed-controlled system remains asymptotically stable as long as all characteristic roots have negative real parts. As the time delay increases and reaches the critical value $\tau_{\max}$, a pair of complex-conjugate characteristic roots may cross the imaginary axis. Under the transversality condition, this root crossing induces a Hopf bifurcation, leading to the onset of oscillatory instability. Therefore, the stability region of the controller is defined by

$$0 < \tau < \tau_{\max}. \tag{66}$$

Furthermore, since $|\sin(\omega\tau)| \leq 1$, and $|\cos(\omega\tau)| \leq 1$, Equation (63) yields the admissibility condition on the feedback gain

$$K \geq \max\left(\frac{\omega_c^2 - \lambda_i}{2},\ |\mu_i|\,\omega_c\right). \tag{67}$$

Equations (66) and (67) explicitly define the stability region in the (K,τ) parameter space by determining the critical delays, admissible feedback gains, and delay margins. Consequently, they provide a rigorous analytical basis for the design, tuning, and robustness evaluation of the proposed delayed feedback controller.

4.3.3. Numerical verification

Figure 14 illustrates the temporal evolution of the system response under the same parameters as in **Figure 12**, comparing the uncontrolled (black) and controlled (red) configurations. The introduction of the controller significantly modifies the system's dynamic behaviour. While the uncontrolled response exhibits persistent oscillations with noticeable amplitude fluctuations, the controlled curve exhibits a significant attenuation of vibration amplitudes. This demonstrates that the control gain effectively dissipates the system's energy, reducing oscillatory effects and stabilizing the motion over time. The smooth decay of the red curve indicates that the selected control parameters ensure an overdamped or slightly underdamped regime, confirming the efficiency of the proposed feedback strategy in enhancing dynamic stability.

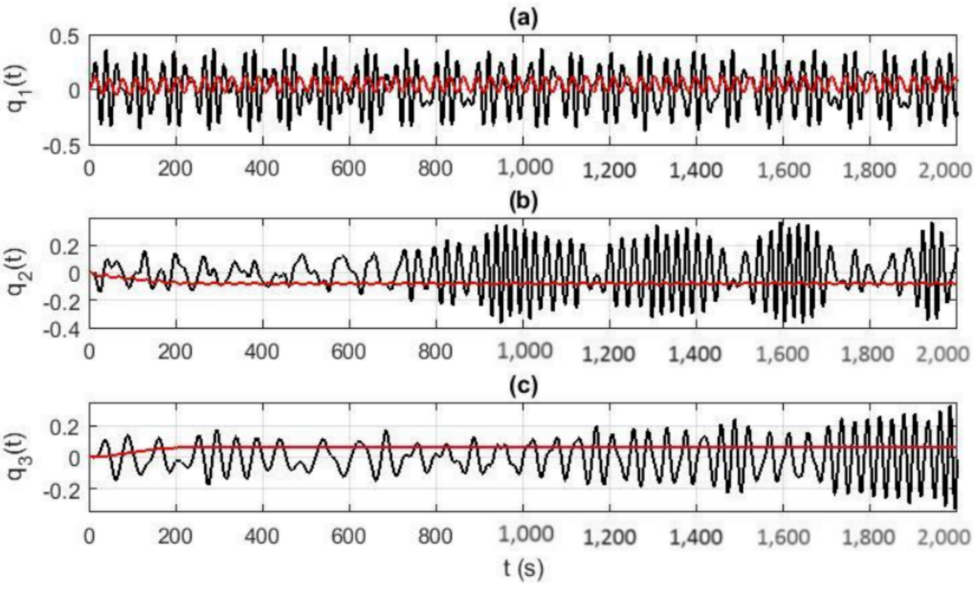

Figure 14. Temporal evolution obtained for the parameters as in **Figure 12**.
Note: Black: without controller. Red: with the controller with $K = 0.08$, and $\tau = 5$.

4.4. Discussion

The results demonstrate that the dynamic response of multilayer beam-soil systems is highly sensitive to excitation and foundation parameters. The equilibrium diagrams and frequency-response curves reveal multistability, resonance amplification, and branch-jump phenomena, which are typical signatures of strongly nonlinear systems. Similar sensitivity of the dynamic response to soil properties and moving-load conditions has been reported by Gao et al. and Li et al. [22, 23] for multilayer soil systems subjected to moving excitations.

The nonlinear frequency-response curves obtained in **Figures 3** and **4** exhibit resonance peaks, hysteresis regions, and multiple coexisting solution branches. These observations are consistent with the resonance amplification mechanisms reported by Ai and Wang and Banushi and Soga [24, 25] for beam-soil systems resting on compressible foundations. The enlargement of the multistability regions with increasing excitation levels further highlights the important role of nonlinear effects in governing the vibration response.

The comparison between the two-layer and three-layer configurations shows that increasing the number of layers considerably enriches the system dynamics. Additional degrees of freedom promote energy transfer between layers and generate more complex resonance patterns. This observation agrees with the findings of Lee and Fan et al. [26,27], who showed that multilayer beam configurations significantly modify the dynamic characteristics of the structure.

The numerical simulations also reveal the importance of interlayer coupling in shaping the vibration response. The appearance of additional frequency components and the redistribution of vibration energy among the layers are consistent with the conclusions of Zhou et al. [28], who emphasized the critical role of coupling stiffness and damping in multilayer systems subjected to moving loads.

Furthermore, the observed influence of the beam-soil interaction on vibration amplitudes and modal behaviour is in qualitative agreement with the studies of Ma et al. [29, 30] and Wang et al. [31], which reported that foundation characteristics strongly affect the dynamic response and resonance behaviour of structures resting on deformable soils.

Finally, the proposed delayed feedback controller effectively suppresses vibration amplitudes and improves the dynamic stability of the system. The controlled responses exhibit a clear attenuation of oscillations compared with the uncontrolled case, demonstrating the potential of time-delay control strategies for mitigating excessive vibrations in multilayer beam-soil systems subjected to moving loads.

5. Conclusion

This study developed a comprehensive nonlinear dynamic model for multilayer beams resting on compressible clayey soil and subjected to a moving concentrated force. The formulation was established using a Lagrangian framework that incorporates bending energy, interlayer coupling, Winkler-type soil stiffness, damping, and geometric nonlinear stretching effects. By applying modal reduction, the distributed dynamic model is converted into a reduced-order system of coupled Duffing-type nonlinear equations governing the dynamic response of the layered beam.

The analytical and numerical investigations demonstrated that the dynamic response of the system is strongly influenced by interlayer coupling parameters, soil compressibility, excitation frequency, and nonlinear stiffness coefficients. The results revealed complex behaviours, including resonance amplification, multistability, quasi-periodic motion, and branch-jump phenomena. These nonlinear effects highlight the sensitivity of multilayer beam-soil systems to parameter variations and confirm the necessity of nonlinear modeling in transport and infrastructure applications subjected to moving loads.

To improve dynamic stability, a time-delay feedback controller was introduced and applied to all modal coordinates. The delayed control law led to a transcendental characteristic equation, from which explicit stability conditions were derived in terms of the feedback gain and time delay. Numerical simulations showed that the proposed delayed feedback strategy effectively attenuates oscillations, suppresses nonlinear amplification, and accelerates convergence toward equilibrium. The results confirm that delay-based control can significantly enhance the stability of multilayer structural systems subjected to dynamic excitation.

Overall, this work contributes to the theoretical understanding of nonlinear soil-structure interaction in multilayer systems and demonstrates the effectiveness of time-delay feedback control in mitigating vibration instabilities.

Future research should naturally build upon the limitations of the present formulation while preserving its analytical framework. Although the nonlinear Winkler foundation adopted in this study provides an efficient representation of beam–soil interaction, it neglects the shear interaction between adjacent soil elements. Future work will therefore focus on extending the present formulation to more refined foundation representations capable of incorporating this interaction in order to improve the prediction of vibration transmission and load redistribution in compressible clayey soils. Furthermore, the current model relies on a single-mode Galerkin approximation, which is appropriate because the fundamental mode dominates the structural response under the loading conditions investigated. Nevertheless, higher-order vibration modes may become increasingly important under stronger excitations or over wider frequency ranges. Future investigations will therefore consider multimodal Galerkin formulations to quantify their influence on resonance amplitudes, modal interactions, and the overall dynamic behaviour of multilayer beam systems. In addition, the numerical results obtained in this work have revealed several nonlinear phenomena, including multistability, resonance amplification, branch-jump phenomena, and quasi-periodic oscillations. A more systematic exploration of these behaviours through an extended parametric analysis will provide a better understanding of the stability boundaries and the transition mechanisms between different dynamic regimes as the excitation frequency, coupling stiffness, damping, and time-delay parameters vary. From the control perspective, the effectiveness of the proposed time-delay feedback strategy will be further assessed over a broader range of operating conditions in order to identify combinations of feedback gain and delay that maximize vibration attenuation while maintaining closed-loop stability. Finally, although the proposed analytical model has been supported by extensive numerical simulations, additional validation against finite element simulations performed under identical mechanical and geometric conditions will help establish the range of applicability and predictive capability of the reduced-order formulation. These developments are expected to strengthen the reliability of the proposed modelling framework and facilitate its application to multilayer engineering structures, including railway tracks, bridge decks, industrial platforms, and other beam-supported infrastructures subjected to moving dynamic loads.

Author contributions: Conceptualization, RE and FK; methodology, RE and FK; formal analysis, RE, GHP, HJOB and EEN; investigation, RE, EEN, DTN, JMB and SN; numerical investigation, RE, EEN, DTN and JMB; validation, FK and SN; writing—original draft preparation, RE and FK; writing—review and editing, FK and RE; supervision, FK and SN. All authors have read and agreed to the published version of the manuscript.

Funding: This work received no external funding.

Institutional review board statement: Not applicable.

Informed consent statement: Not applicable.

Data availability statement: The data used in this study are available from the corresponding author upon reasonable request.

Conflict of interest: The authors declare no conflict of interest.

AI use statement: During the preparation of this manuscript, the authors used ChatGPT (OpenAI) solely for language editing, grammar correction, and improvement of readability. No AI tools were used for data collection, data analysis, interpretation of results, scientific reasoning, or generation of scientific conclusions. All AI-assisted outputs were carefully reviewed, verified, and edited by the authors. The authors take full responsibility for the accuracy, integrity, and originality of the content presented in this work.

References

1. Elhuni H, Basu D. Novel nonlinear dynamic beam-foundation interaction model. Journal of Engineering Mechanics. 2021; 147(4): 04020139. doi: 10.1061/(ASCE)EM.1943-7889.0001915
2. Eno R, Wokwenmendam ML, Ndombou GB, et al. Dynamics of a nonlinear multilayer beam structure on elastic foundation: Chaos detection and application to transport engineering technologies. Mathematics and Systems Science. 2025; 3(1): 3058. doi: 10.54517/mss3058
3. Karami B, Ghayesh MH. Moving load excited dynamics of multi-layered imperfect microplates based on various micromechanical models. International Journal of Engineering Science. 2024; 197: 104017. doi: 10.1016/j.ijengsci.2024.104017
4. Li R, Ding R, Hozuri A. Nonlinear vibrations of multiscale composite beams on a nonlinear softening foundation. European Journal of Mechanics—A/Solids. 2023; 100: 104993. doi: 10.1016/j.euromechsol.2023.104993
5. Ter-Martirsyan ZG, Ter-Martirsyan AZ, Sobolev ES. Vibration of embedded foundation at multi-layered base taking into account non-linear and rheological properties of soils. Procedia Engineering. 2016; 153: 747–753. doi: 10.1016/j.proeng.2016.08.237
6. Mourya VK, Pandey G, Patel D, et al. Approaches considering non-linearity in soil-foundation-interaction: A state-of-the-art review. Research on Engineering Structures and Materials. 2023; 9(3): 989–1013. doi: 10.17515/resm2023.646me0117
7. Zhai Z, Yang Y, Wang Y. Element-lumped-based beam vibration modelling with multi-flexible constraints and

implementation into nonlinear train-track-bridge interactions. Nonlinear Dynamics. 2025; 113(1): 19335–19375. doi: 10.1007/s11071-025-11068-5
8. Youzera H, Selim Saleh MM, Ghazwani MH, et al. Nonlinear damping and forced vibration analysis of sandwich functionally graded material beams with composite viscoelastic core layer. Mechanics Based Design of Structures and Machines. 2024; 52(7): 4191–4210. doi: 10.1080/15397734.2023.2229911
9. Kampitsis AE, Sapountzakis EJ. Dynamic analysis of beam-soil interaction systems with material and geometrical nonlinearities. International Journal of Non-Linear Mechanics. 2017; 90: 82–99. doi: 10.1016/j.ijnonlinmec.2017.01.007
10. Poudel N, Chaulagain H. Numerical investigation of nonlinear soil-structure interaction effects on response of irregular RC buildings. Results in Engineering. 2024; 22: 102161. doi: 10.1016/j.rineng.2024.102161
11. Wu CP, Yeh ST, Liu JH. A nonlinear free vibration analysis of functionally graded beams using a mixed finite element method and a comparative artificial neural network. Journal of Composites Science. 2023; 7(6): 229. doi: 10.3390/jcs7060229
12. Rezvykh A. Kyzylorda province, Kazakhstan, April 29, 2012: Construction of Western Europe–Western China road. Caterpillar Asphalt Compactor Flattens Asphalt Layers. Alamy; 2012. Available online: https://www.alamy.com/kyzylorda-province-kazakhstan-april-29-2012-construction-of-west-europe-west-china-road-caterpillar-asphalt-compactor-flatten-asphalt-layers-image551303356.html?imageid=9EF77F33-3EE4-4125-9F78-E3A64944F51A&pn=1&searchId=6e640d0b636c468884bfba6f36b6acaa&searchtype=9
13. Kenmogne F, Noah PMA, Dongmo ED, et al. Effects of time delay on the dynamics of nonlinear beam on elastic foundation under harmonic moving load: Chaotic detection and its control. Journal of Vibration Engineering & Technologies. 2022; 10: 2327–2346. doi: 10.1007/s42417-022-00579-9
14. Kenmogne F, Ouagni MST, Simo H, et al. Effects of time delay on the dynamical behaviour of nonlinear beam on elastic foundation under periodic loadings: Chaotic detection and its control. Results in Physics. 2022; 35: 105305.
15. Junker RG, Relan R, Madsen H. Physical-stochastic continuous time identification of a forced Duffing oscillator. ISA Transactions. 2022; 126: 226–234.
16. Salas AH, Abu Hammad M, Alotaibi BM, et al. Analytical and numerical approximations to some coupled forced damped Duffing oscillators. Symmetry. 2022; 14(11): 2286.
17. Winkler E. The Theory of Elasticity and Strength with Special Consideration of Their Application in Engineering for Polytechnic Schools, Building Academies, Engineers, Mechanical Engineers, Architects, etc. Dominicus; 1867. (in German)
18. Amabili M. Nonlinear Vibrations and Stability of Shells and Plates. Cambridge University Press; 2008.
19. Timesli A. Buckling behaviour of SWCNTs and MWCNTs resting on elastic foundations using an optimization technique. Physical Mesomechanics. 2022; 25: 129–141.
20. Salas Salas AH, Castillo Hernández JE, Martínez Hernández LJ. The Duffing oscillator equation and its applications in physics. Mathematical Problems in Engineering. 2021; 1: 9994967.
21. Michiel W, Niculescu SI. Stability and Stabilization of Time-Delay Systems: An Eigenvalue-Based Approach. Society for Industrial and Applied Mathematics (SIAM); 2007. doi: 10.1137/1.9780898718645
22. Gao G, Chen J, Yang J, et al. Field measurement and FE prediction of vibration reduction due to pile-raft foundation for high-tech workshop. Soil Dynamics and Earthquake Engineering. 2017; 101: 264–268.
23. Li D, Yang H, Ma J, et al. Analytical investigation on the dynamic behaviour of multi-span continuous beams supported on soil with finite depth. Coatings. 2024; 14(7): 864. doi: 10.3390/coatings14070864
24. Ai ZY, Wang LH. Effect of compressible parameters on vertical vibration of an elastic pile in multilayered poroelastic media. Computers and Geotechnics. 2017; 89: 195–202. doi: 10.1016/j.compgeo.2017.05.002
25. Banushi G, Soga K. Transition frequencies and dynamic amplification of buried lifelines: A semi-analytical Timoshenko beam on Winkler foundation model. arXiv Preprint. 2025. doi: 10.48550/arXiv.2509.16906
26. Lee JW. Free Vibration Analysis of Three Layered Beams with a Soft-Core Using the Transfer Matrix Method. Applied Sciences. 2023; 13(1): 411. doi: 10.3390/app13010411
27. Fan H, Zhang J, Zheng J. Dynamic response of a three-dimensional multi-layered pavement system subjected to a moving load. Soil Dynamics and Earthquake Engineering. 2022; 160: 107358. doi: 10.1016/j.soildyn.2022.107358
28. Zhou W, Wu L, Jiang L, et al. Research on dynamic response of multi-layer beam system considering random interlayer parameters. Journal of Vibration and Control. 2023; 29(7–8): 1862–1873. doi: 10.1177/10775463211072628
29. Ma J, Wang J, Wang C, et al. Vibration response of beams supported by finite-thickness elastic foundation

under a moving concentrated force. Journal of Mechanical Science and Technology. 2024; 38: 595–604. doi: 10.1007/s12206-024-0108-y

30. Ma J, Yang H, Li D, et al. Vibration response of a finite-length beam on a modified Winkler foundation subjected to moving force groups. Journal of Mechanical Science and Technology. 2025; 39: 3743–3754. doi: 10.1007/s12206-025-0601-y
31. Wang Y, Zhu X, Lou Z. Dynamic response of beams under moving loads with finite deformation. Nonlinear Dynamics. 2019; 98: 167–184. doi: 10.1007/s11071-019-05180-6